

Interpretation of time-lapse seismic data from a heavy oil field, Alberta, Canada

Byron Matthew Kelly and Donald C. Lawton

ABSTRACT

Two 3-D seismic datasets and their difference volume were interpreted and analyzed for the presence of amplitude anomalies and time delays related to the injection of steam into a shallow, heavy oil reservoir. High amplitude anomalies were observed on the monitor data in conjunction with apparent time-thickening of the reservoir interval due to a decrease in the P-wave velocity. The decrease of velocity was interpreted to be due to the increase in reservoir temperature and decrease in differential pressure created from the injection of high temperature steam into the McMurray Formation reservoir. An analysis of the amplitude anomalies yielded a spatial display of reservoir steam chamber distributions.

The attenuation of high frequencies beneath steam chambers was observed within the monitor survey, characterized by low-frequency shadows, observable on the Devonian reflection underlying the amplitude anomalies.

Geological well log information was integrated with the geophysical observations. McMurray Formation channels sands were observed within the seismic data through the analysis of the semblance attribute, as well as within the geological data as low gamma ray values on well log cross sections. The channel sands were observed to intersect amplitude anomalies with the monitor volume. Outside of the amplitude anomalies, the channel sands were bound by muddy IHS bedding, creating baffles to steam flow.

INTRODUCTION

Time-lapse monitoring is comprised of a baseline survey, ideally recorded before the onset of production, and a monitor survey recorded after a period of oil, gas or water production (Clifford, et al., 2003; Kalantzis, 1996). The objective of time-lapse seismic monitoring is to image production induced changes within the reservoir and to identify areas of bypassed reserves, or regions in which current steam injection is not optimally stimulating reserves. The analysis of monitor surveys may allow for the detection of both large and subtle changes within the reservoir (Johnston, 1997). To aid in the time-lapse interpretation, a difference volume was produced through the subtraction of the baseline data from the monitor data, producing a third dataset comprised of traces that are different between surveys. Difference volumes form the foundation for time-lapse seismic analysis, ideally integrated with reservoir characterization, geological modeling and reservoir production (Johnston, 1997).

The 4D dataset analyzed in this study is an ideal candidate for time-lapse interpretation. The baseline survey was recorded prior to production and possesses a high S:N ratio, while the monitor survey was recorded after nine years of steam injection and production. The monitor data contains steam chambers and elevated temperatures within the reservoir zone, albeit a lower S:N ratio due to noise contamination from production

and surface activities. The strong contrast between the ideal baseline survey and a production influenced monitor survey has allowed for a detailed interpretation of reservoir changes due to production to be made.

However, observable time-lapse differences are a result of multiple factors, in which reservoir changes are one of many constituents. Differences in survey acquisition, processing, and near surface velocities during data acquisition can reduce the repeatability of a monitor survey, altering the phase, amplitude and static solution between surveys. The monitor survey was calibrated to match the phase, amplitude and statics to those of the baseline, effectively enhancing production-induced changes while suppressing differences created by other factors. Section 4.4 addresses the calibration procedure that was applied to the dataset.

Following calibration, the baseline, monitor, and difference volumes were interpreted for reservoir changes, identifying heated reservoir intervals and correlating these observations to well logs and production data.

INTERPRETATION OVERVIEW

The interpretation of the 4D P-wave data is focused on production induced changes occurring within the McMurray Formation reservoir. The McMurray reservoir lies below the Clearwater C reflection (cap rock for the reservoir) and above the Devonian Carbonate reflection (Paleozoic unconformity). Time delays are observed along the Devonian reflection (monitor) due to a reduction in P-wave velocity of the heated bitumen sands in the overlying McMurray reservoir (see section 1.3, Chapter 1). These velocity anomalies, in combination with seismic attributes, reservoir isochrons, and amplitude anomalies, were that target of the P-wave 4D interpretation.

The interpretation of the time-lapse seismic did not include the data within the vicinity of the Quaternary channel. As discussed in Chapter 2 (section 2.3), the Quaternary channel infill is highly attenuative, preventing coherent imaging of the Quaternary channel boundaries and the underlying reflections (Figure 2-7, Chapter 2). Thus, all seismic underlying the Quaternary channel was considered to be low quality and unreliable data, and was not considered during the time-lapse interpretation.

Prior to the interpretation of the time-lapse dataset, both the baseline and monitor data were bulk shifted to later times by 250ms to tie the data into other interpretations and well logs. Although this thesis will not address these additional interpretations, it is important to take note of the bulk shift when comparing images of the data in this chapter to those in Chapter 3.

DATA COMPARISON

Despite the best efforts to process the data in an identical manner, there are some differences in the baseline and monitor data. Figure 1 is a comparison of the baseline and monitor data, taken from the center of the survey within an area of known steam injection. A comparison of the shallow reflections displays the large S:N and phase

disparity between the baseline and monitor data. Globally, there is a phase difference of 34 degrees between the two datasets, as well as a discrepancy in the amplitudes of the higher frequencies (Figure 2). Overall, the baseline data is of higher quality than the monitor data.

The color overlay on the monitor data is the amplitude difference between the two datasets, calculated by subtracting the baseline data from the monitor data. Positive differences are yellow and negative differences are green-orange. There are a large number of differences that due to disparity in phase, statics and amplitudes, as well as differences within the reservoir due to production. Through the calibration procedure, section 4.5, non-production induced differences will be reduced, while steam related anomalies will be preserved.

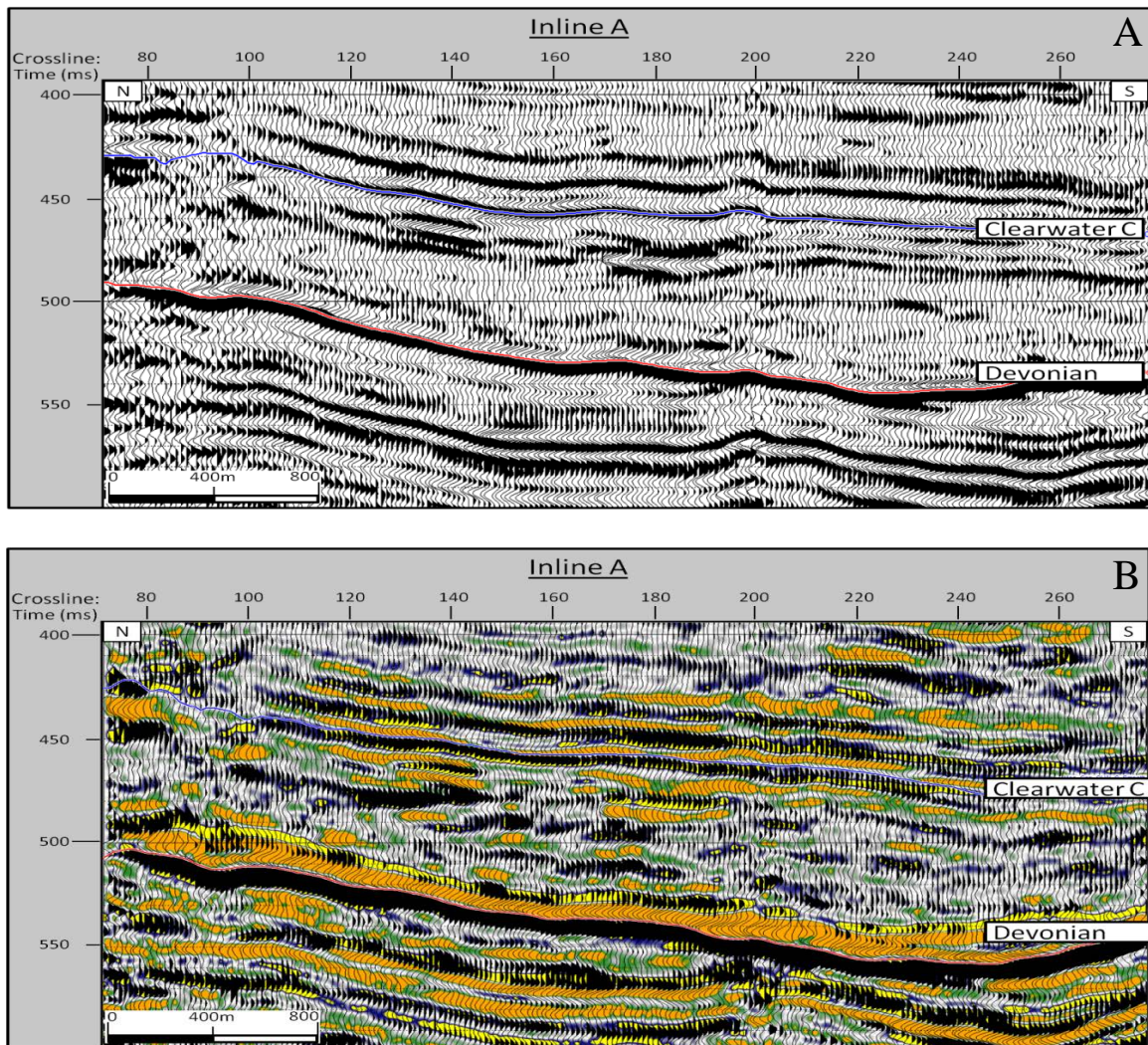


Figure 1 A comparison of (a) 2002 baseline survey to (b) 2011 monitor survey before calibration. The overlay color is the amplitude difference between the baseline and monitor data, calculated by subtracting the baseline data from the monitor data.

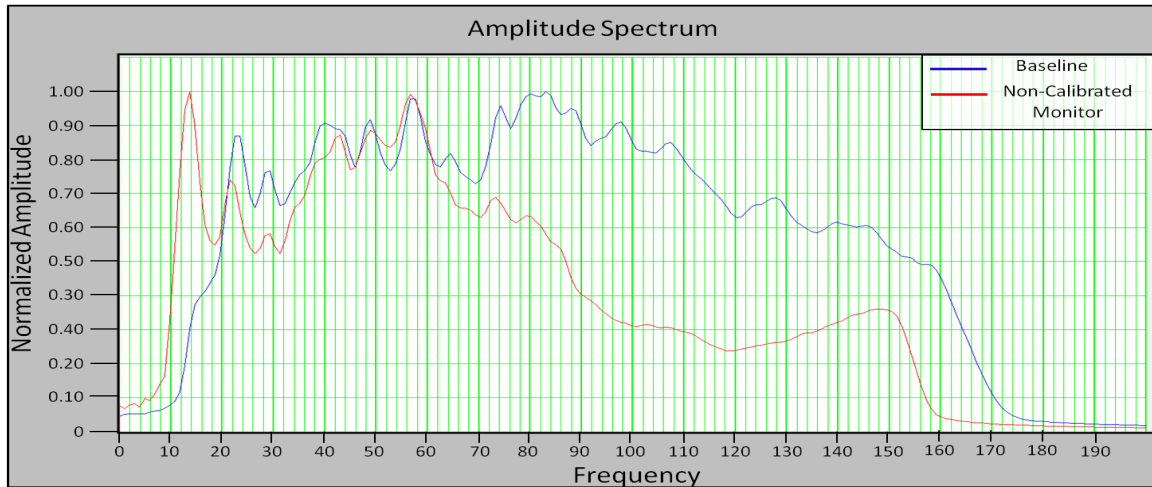


Figure 2 Amplitude spectrum for all traces in the baseline and monitor data before calibration. There is a large discrepancy in the amplitudes of the high frequencies (70-160 Hz).

Normalized RMS

To provide a detailed understanding of the differences between the baseline and monitor survey, NRMS difference maps, crosscorrelation maps and time-shift maps of the reservoir interval were produced. NRMS difference maps are constructed by taking the difference between the two datasets on a sample-by-sample basis, with RMS equalization of the amplitudes prior to the difference calculation as follows:

$$NRMS = \frac{2 * RMS (B - A)}{RMS (A) + RMS (B)} \quad 1$$

where A is the baseline survey and B is the monitor survey, and where the RMS operator is defined as (Kragh & Cristie, 2002):

$$RMS = \sqrt{\frac{\sum_{t_1}^{t_2} (x_t)^2}{N}} \quad 2$$

where N is the number of samples in the interval of t_1 - t_2 .

NRMS is a measure of the difference between the two surveys over a specified interval, normalized to a value ranging from 0-200 percent, where zero percent represent identical data and 200 percent represents totally uncorrelated data (Sheriff, 2002; Kragh & Cristie, 2002). NRMS is largely affected by small differences within the data, including noise, phase shifts and amplitude differences (Kragh & Cristie, 2002). Hence, NRMS provides a good display of the overall difference between two datasets.

Typical NRMS values are in the range of 10-30% after calibration, but may often exceed this due to acquisition and repeatability issues. For example, Koster, et al., (2000) displayed average NRMS values of 35% in the Draugen field, while Kommedal, et al.,

(2005) reported NRMS values of 14% and Eiken, et al., (2003) quoted NRMS values as low as 6-12%.

Figure 3a is an NMRS map taken above the Clearwater C horizon within an area free of reservoir production. The NRMS map displays areas of relatively lower value (80 percent) as well as areas of higher NRMS value (1.80 percent). Overall, the NRMS value is high, signifying that considerable differences exist between the two surveys that are not related to production. Through the calibration procedure, (section 4.5), the overall NRMS value is reduced through adjustments made to the monitor survey in terms of phase, statics (time shifts) and amplitudes.

Figure 5a is an NRMS map for the Devonian interval. The NRMS map displays areas of relatively lower NRMS value (100 percent) and areas of high NRMS value (1.90 percent), suggesting that considerable differences exist between the baseline and monitor survey.

Crosscorrelation

Crosscorrelation maps provide an understanding of the correlativity of two datasets, where similar or identical events will have a high correlation values and dissimilar or unique events (i.e. Events only observed on the monitor survey) will have a low correlation value. Crosscorrelation is a simple signal processing technique where a stationary or reference trace (baseline) is matched to a corresponding sliding trace from the input (monitor) over a specified time window. Computed crosscorrelation maps are interpreted in conjunction with computed time-shift maps, where time-shift maps display the shift (or lag) in ms required to produce the corresponding crosscorrelation values. Crosscorrelation and time-shift values are computed in conjunction; the amplitude value for two traces (baseline and monitor) are multiplied together and summed to produce a total value for the initial lag, following which the trace is shifted down one sample and a new value is computed (dot product). Using the initial alignment as the zero lag position, a plot of lag vs. dot product displays the best time-shift required to produce the maximum dot product, or the highest normalized crosscorrelation values (Figure 6) (Yilmaz, 2001; Gadallah, 2005). These time-shift values provide an understanding of the static adjustments required to better align the reflections in time. Examples of the application of crosscorrelation are given by Eastwood et al., (1998) and Drijkoningen et al., (2012).

Figure 3(b) is a crosscorrelation map produced over the same interval as the NRMS map, and Figure 3(c) is the corresponding time-shift map. The overall crosscorrelation value is high for this interval (70-90 percent), indicating that the cap rock reflections of the monitor survey correlate well with those of the baseline survey. However, to produce this high correlation, each trace must be shifted by a corresponding time-shift values as displayed in Figure 3(c), ranging from -8.0 to +6.0 ms. These time-shifts were later corrected through the calibration procedure as both a global correction and as a trace-by-trace correction.

Figure 4 and Figure 5 display crosscorrelation and time-shift values for the McMurray Formation reservoir and the Devonian interval. Again, considerable differences are observed, due to discrepancies between the baseline and monitor surveys.

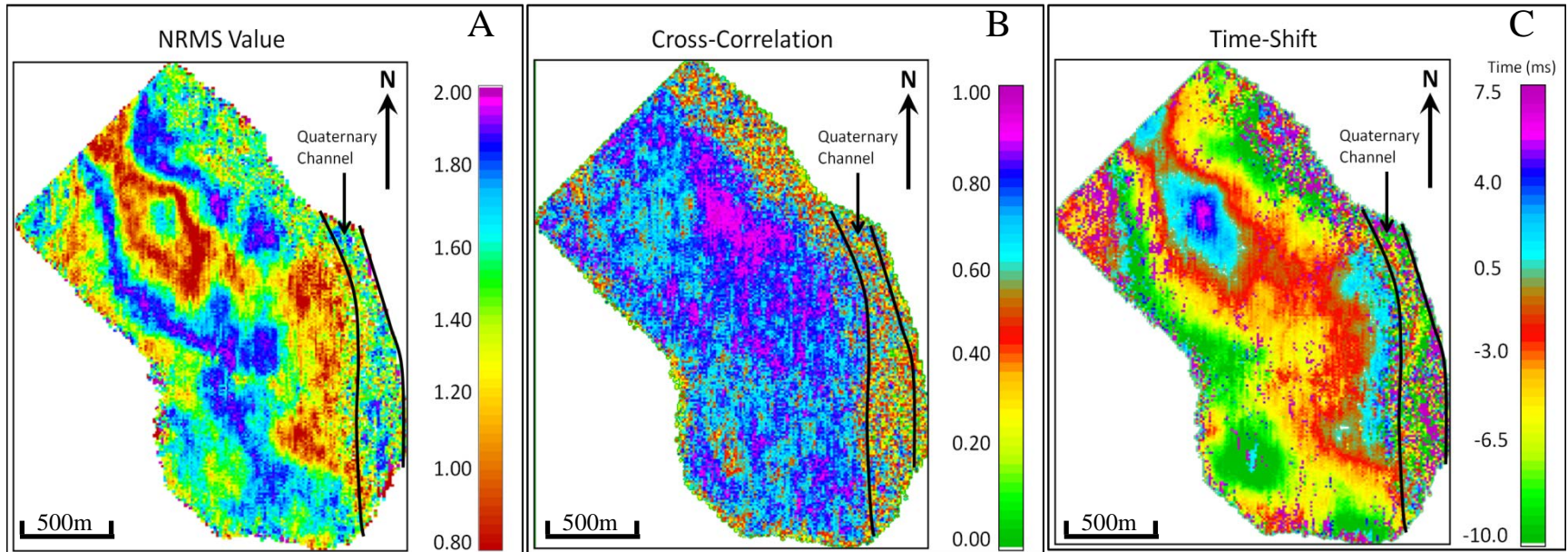


Figure 3 (a) NRMS error map of the Clearwater C interval, an area free of reservoir production (35ms window beginning 35ms above the Clearwater baseline horizon) (b) Crosscorrelation map and (c) Time-shift map of the same interval. The NRMS map displays areas of relatively low NRMS value (80 percent) and areas of high NRMS value (1.80 percent), suggesting that considerable differences exist between the baseline and monitor survey in terms of phase, amplitudes and statics. The crosscorrelation map shows overall high correlation values (0.70 - 0.90) which correspond to time-shift values of -8.0 to +6.0 ms. The high correlation suggests that significant time-shifts are required to align the cap rock reflections of the monitor survey with those of the baseline, which would produce an overall high correlation. The outlined quaternary channel to the east represents a region of unreliable data due to signal attenuation from the Quaternary channel infill.

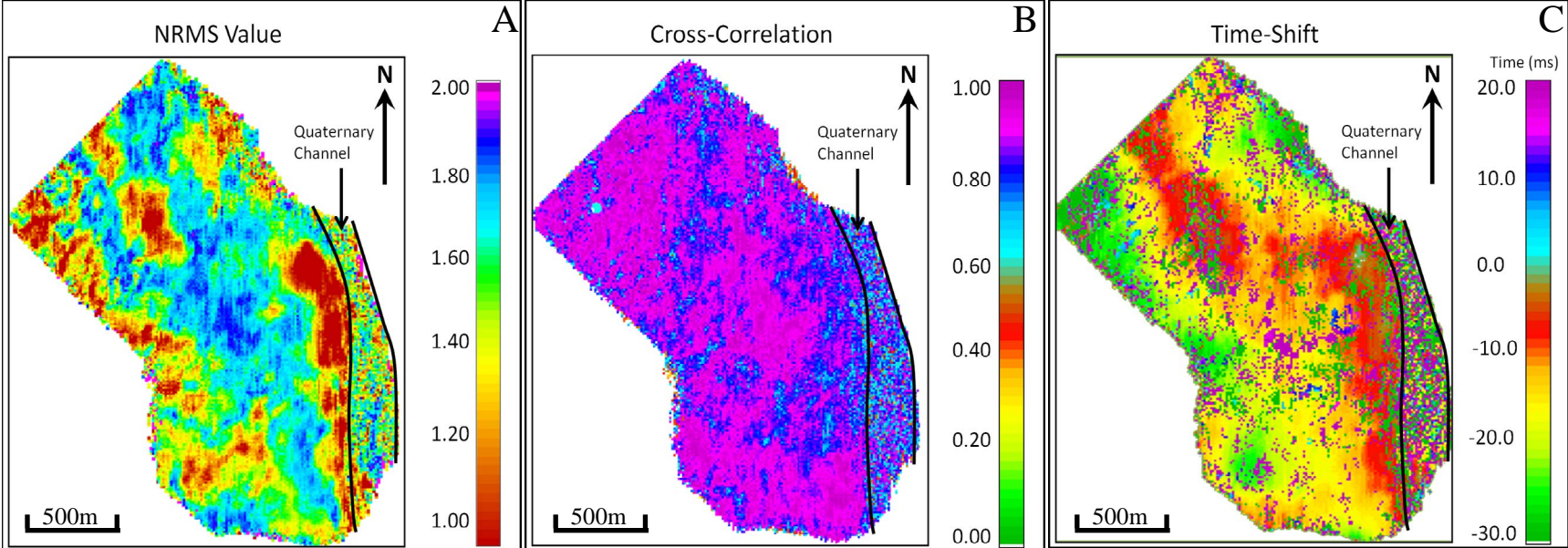


Figure 4 (a) NRMS error map of the Devonian interval (70ms window beginning 20ms above the zero crossing of the Devonian horizon) (b) Crosscorrelation map and (c) Time-shift map of the same interval. The NRMS map displays areas of relatively low NRMS value (100 percent) and areas of high NRMS value (1.90 percent), suggesting that considerable differences exist between the baseline and monitor survey in terms of phase, amplitudes and statics. The crosscorrelation map (b) shows overall high correlation values (0.80 - 1.00) which correspond to time-shift values of --30.0 to +20.0 ms. The high correlation suggests that significant time-shifts are required to align the cap rock reflections of the monitor survey with those of the baseline, which would produce an overall high correlation. The outlined quaternary channel to the east represents a region of unreliable data due to signal attenuation from the Quaternary channel infill.

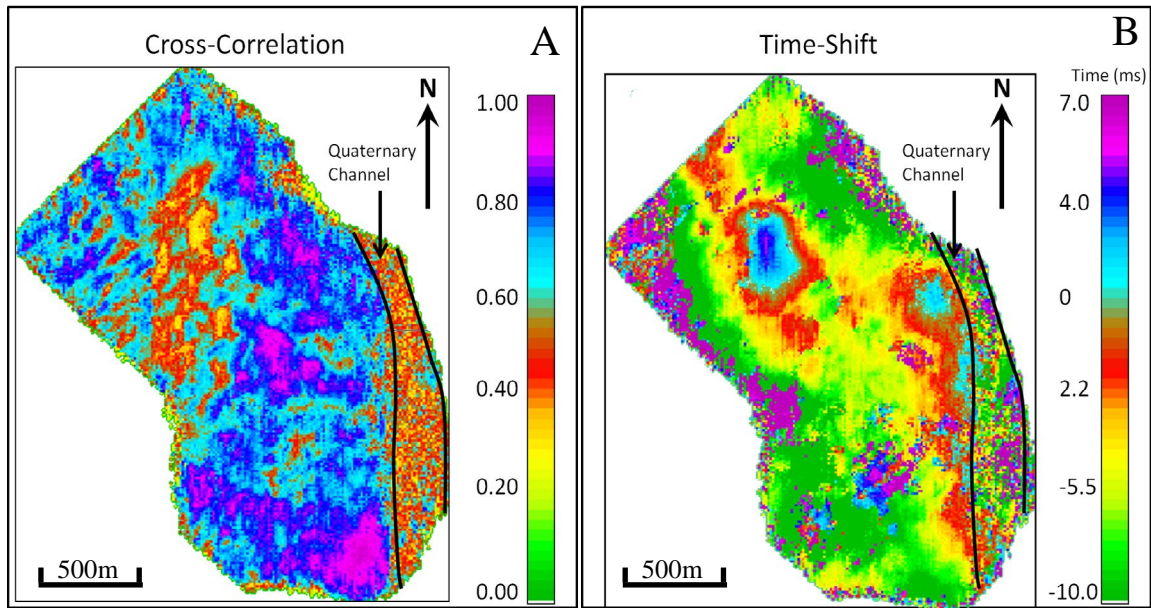


Figure 5 (a) Crosscorrelation map of the McMurray Formation reservoir interval (Clearwater C reflection to the Devonian reflection) and (b) Time-shift map of the same interval. The crosscorrelation map shows overall high correlation values (0.60 - 0.70) as well as an area of low correlation value (0.30-0.50) Time-shift values range from 7.0 to - 10.0 ms. Regions exhibiting large time-shift values correlate low crosscorrelation values, and correlate with known reservoir steam injection. The outlined quaternary channel to the east represents a region of unreliable data due to signal attenuation from the Quaternary channel infill.

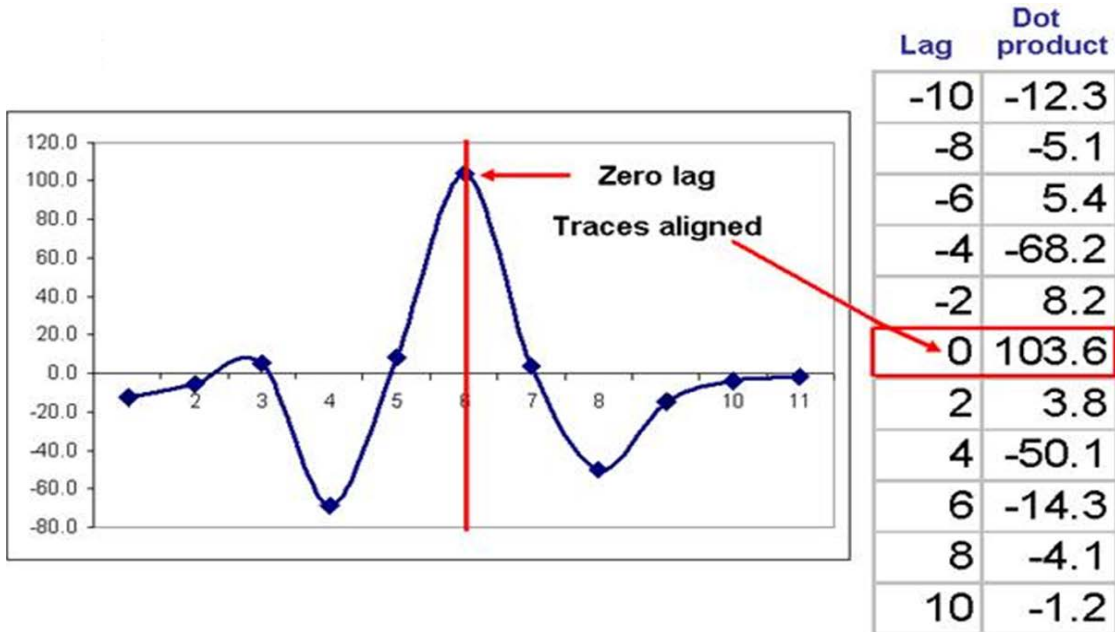


Figure 6 Plot of lag vs. dot product for some theoretical set of traces. In this example, a time-shift of 0 ms is required to produce the maximum crosscorrelation value (Taken from Hampson-Russell's Pro4D guide).

HORIZON INTERPRETATION

Prior to interpretation, the temporal positioning of the reservoir and reflectors of interest was determined. The main geological units of interest, as discussed in chapter 2 (section 2.2), are represented as seismic horizons corresponding to the Devonian Carbonates of the Beaverhill Lake Group, the Clearwater B Formation, and the Clearwater C Formation (cap rock). Each horizon was identified within the seismic data through the correlation of seismic reflections with geological units, where geological well tops identified on sonic logs were related to seismic reflectors via synthetic seismograms. The synthetic seismograms were generated by the convolution of the reflectivity series with an Ormsby wavelet containing a frequency range representative of that within the data. Figure 7 is an example of a synthetic seismogram tie for well A displaying well log tops for the Devonian, and Clearwater C Formations, and their relationship to the seismic data. Following the well tie, seismic horizons were picked on the zero crossing for each reflector of interest. Horizons were initially picked on the baseline survey and non-calibrated monitor survey, and after data calibration, repicked on the monitor survey (see section 4.4.4). For more information about the seismic characteristic of each reflector of interest, refer to section 2.2 (Chapter 2).

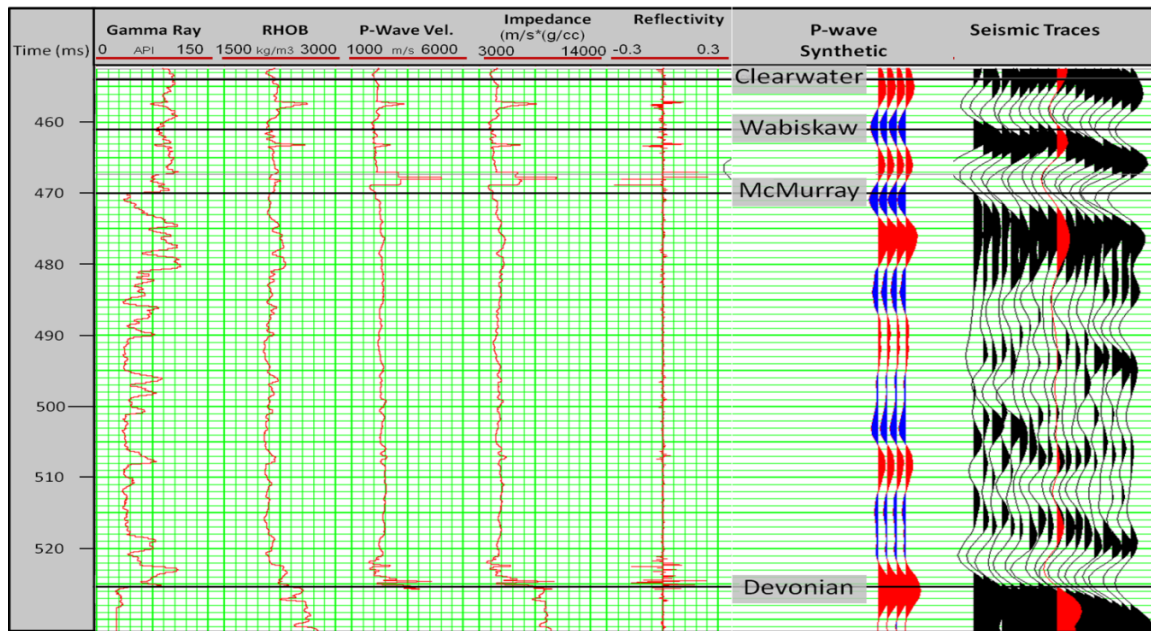


Figure 7 Synthetic seismogram for well A from the center of the survey area, including the calculated impedance and reflectivity for the Clearwater and Devonian reflections. The red trace is the reference trace from the seismic data.

PRELIMINARY INTERPRETATION

Before data calibration, a preliminary interpretation of the baseline and non-calibrated monitor survey was performed to gain an understanding of amplitude anomalies observable within the reservoir interval. The interpretation of this time-lapse dataset was focused on the McMurray Formation reservoir, lying between 450-550 ms, bound above by the Clearwater C horizon and below by the Devonian horizon.

Figure 8 is a seismic cross section taken along an arbitrary line running NW to SW through both the baseline and non-calibrated monitor data, focused on the McMurray Formation reservoir. Between inlines 160 and 180, at a time of 500 - 510 ms on the monitor survey, we observe a high amplitude event which is not observed on the baseline survey. This high amplitude event coincides with a velocity pushdown along the Devonian reflection of 6 ms. Overlaying gamma ray logs onto the baseline and non-calibrated monitor data demonstrates that the high amplitude anomaly intersects a low gamma ray value, representing a channel sand within the Lower McMurray Formation. The intersection of an amplitude anomaly with reservoir channel sands is interpreted to be indicative of a steam induced anomaly.

A second high amplitude event is observed on the non-calibrated monitor data between inlines 100 and 120, at a depth of 530 – 540 ms, which is also not present on the baseline data. This event coincides with a Devonian time delay of 8ms, and intersects Lower McMurray channel sands, as indicated by the low gamma ray values on the overlain log. Again, this amplitude anomaly is interpreted to be due to steam injection.

Both of the amplitude anomalies are bounded by a mud or shaly unit, as indicated by a high gamma ray value overlying each anomaly. This muddy or shaly interval is a baffle

to steam flow, preventing the steam from migrating upward in the reservoir to earlier times. The combination of channel sand with an overlying impermeable unit is representative of a flow conduit for steam within the reservoir. Injected steam will preferentially flow along the pours and permeable channel sands, migrating laterally throughout the reservoir while being bound to lower times due to the overlying baffle. This steam migration will bypass bitumen reserves in overlying channel sands, as steam cannot transfer heat through the shale/mud to the overlying channel sands.

To provide further support for the presence of channels within the McMurray Formation reservoir, the baseline data was transformed into a semblance volume. Semblance is a seismic attribute, used to analyze data for changes in the seismic character, computed by comparing the amplitude of a single trace to that of an adjacent trace.

Semblance is calculated over a 3D analysis window, with a defined dip and azimuth for each point in the data volume (zero dip for a flattened volume) (Marfurt, et al., 1999; Chopra & Marfurt, 2007). Semblance is defined as the ratio of energy of the average trace to the average energy of all the traces along a specified dip, averaged over a specified analysis window. Semblance, $S(t, p, q)$ is defined as follows:

$$S(t, p, q) = \frac{\sum_{k=-K}^K \left[\frac{1}{J} \sum_{j=1}^J u_j(t+k\Delta t - px_j - qy_j) \right]^2}{\sum_{k=-K}^K \frac{1}{J} \sum_{j=1}^J [u_j(t+k\Delta t - px_j - qy_j)]^2} \quad 3$$

where x_j and y_j denote the x and y distances of the j th trace from the center trace, summed over $2K + 1$ samples. P and q are the apparent dips measured in milliseconds per meter and t is the time in milliseconds (Chopra & Marfurt, 2007).

Semblance values range from 0 (low) to 1 (high), where traces exhibiting a semblance of 0 have extremely different amplitudes and traces with a semblance of 1 have the same amplitudes. Effectively, semblance is a quantitative measure of the coherency of seismic data across a set of traces (Chopra & Marfurt, 2008). The semblance attribute is effective at delineating discontinuities that would cause a change in the seismic signal, such as faults or channel edges (Chopra & Marfurt, 2008). Hence, we can use the semblance analysis to identify channels within the McMurray Formation reservoir.

Figure 9a is a time slice through the semblance volume displaying low semblance values (white). These low semblance values are interpreted to be channels within the upper McMurray Formation reservoir.

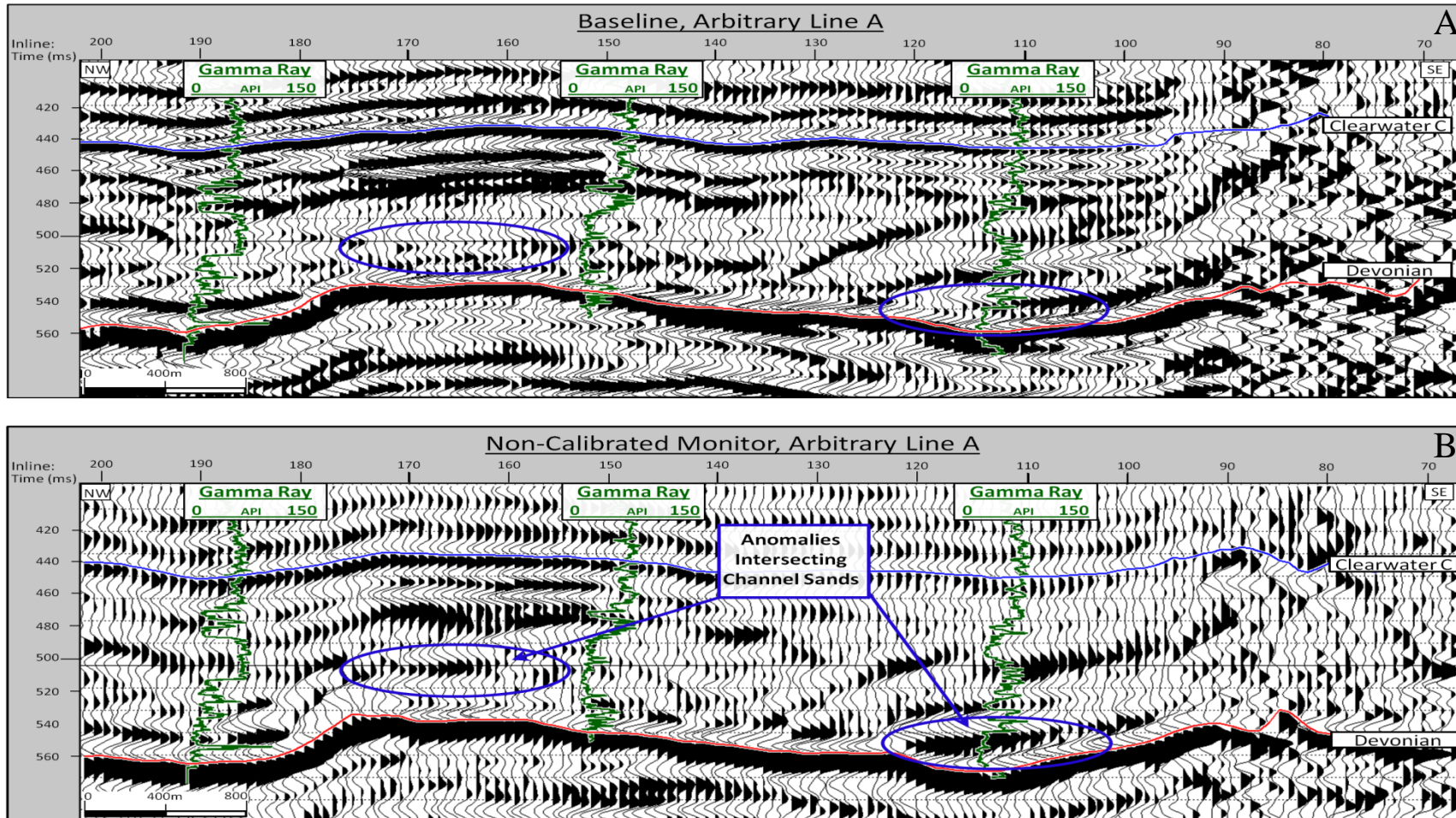


Figure 8 Arbitrary Line A running NW - SW through (a) baseline and (b) non-calibrated monitor data. Two amplitude anomalies are observed on the non-calibrated monitor data. Gamma ray logs indicate the intersection of the anomalies with Lower McMurray Formation channel sands. The anomalies are interpreted to be indicative of steam injection into the McMurray Formation reservoir. Data on the SE end of the line is low quality due to signal attenuation from the Quaternary channel.

Frequency Attenuation

The analysis of the frequency content of the data may be indicative of reservoir steam zones. The attenuation of frequency beneath a steam induced anomaly has been discussed by Hickey, et al., (1991), Isaac (1996) and Yuwen (1998), attributing the attenuation of higher frequencies to a decrease in the viscosity of reservoir pore fluids. Velocity and viscosity are largely influenced by temperature, decreasing considerably during steam injection in conjunction with elevated reservoir temperatures above ambient values. These decreases may lead to high-frequency attenuation, where the frequency content of the reflections underlying steam zones may be characterized by low-frequency shadows (Taner, et al., 1979; Isaac, 1996; Macrides & Kanasewich, 1987). Hence, the non-calibrated monitor data was analyzed for the presence of low-frequency zones underlying observed amplitude anomalies.

Complex seismic trace analysis was employed generate an instantaneous frequency volume to aid in the investigation of low-frequency zones. Instantaneous frequency is the temporal measurement of the rate of change of the instantaneous phase, with respect to time (the time derivative of instantaneous phase; see Appendix A) (Tanner, 2002; Barnes, 2007). Instantaneous frequency is defined as (Barnes, 2007):

$$f(t) = \frac{1}{2\pi} \frac{d\theta(t)}{dt} \quad \mathbf{4}$$

where $\Theta(t)$ is the instantaneous phase (Barnes, 2007):

$$\theta(t) = \arctan \left[\frac{y(t)}{x(t)} \right] \quad \mathbf{5}$$

and where $x(t)$ is the seismic trace and $y(t)$ is the seismic trace rotated by -90 degrees (see section 4.6.3 or Appendix A).

The baseline and non-calibrated monitor data were transformed to instantaneous frequency volumes using Hampson-Russell's Pro4D software. The two amplitude anomalies observed in Figure 8 correspond with a decrease in frequency content of the events underlying each anomaly. Figure 10 is a comparison of the baseline and non-calibrated monitor instantaneous frequency volumes. There is a low frequency shadow observed at 510 ms on the monitor data between inlines 110 and 150, located on the Devonian reflection underlying the amplitude anomaly. To display the spatial distribution of the frequency attenuation, a time slice was taken through the baseline instantaneous frequency volume and the non-calibrated monitor instantaneous frequency volume (Figure 11). These time slices display the instantaneous frequency values, averaged over a 20ms window, beginning 510 ms beneath the anomaly observed between inlines 110 and 150. A comparison of the baseline and non-calibrated monitor frequency values displays the attenuation of higher frequencies on the non-calibrated monitor data, where instantaneous frequency values are significantly lower than those on the baseline data. The blue circle represents of the location of the amplitude anomaly on the time slices.

Other areas of the reservoir displayed significant frequency attenuation, as observed on the non-calibrated monitor instantaneous frequency volume time slice. Overlaying the horizontal SAGD well pairs onto the time slices displays the high correlation of horizontal wells with areas of frequency attenuation. These areas of reservoir frequency attenuation are interpreted to be representative of steam within the Lower McMurray Formation.

DATA CALIBRATION AND DIFFERENCING

The time-lapse seismic surveys were loaded into Hampson-Russell Pro4D to perform reflectivity differencing of the two datasets. Prior to subtraction of the two volumes, we compared and calibrated the data to match phase, amplitude and statics between the surveys in an effort to reduce differences that are not production related. The calibration used the baseline survey as a reference, and altered the phase, statics and amplitudes of the monitor survey to match those of the baseline.

The calibration procedure is a comparison of two datasets, where differences are observed and correction factors are calculated and applied to the monitor survey on the basis of dissimilarity with the baseline data, specified within a windowed segment of the data. Typically, the calibration is windowed on reflections above the reservoir that have not undergone reservoir production to ensure that correction factors do not remove production induced changes (Watson, 2004; Nakayama, 2005; Johnston, 1997). However, due to the very shallow nature of our reservoir, coupled with the low S:N ratio and low event coherency of the shallow data (above the Clearwater C horizon), the shallow portion of the monitor survey was ill-suited for calibration. Instead, the calibration of the time-lapse data was windowed on the Devonian reflection. This reflection was chosen on the basis that (1) it is the most coherent and repeatable reflection within the survey due to its high amplitude nature, and (2) it marks the base of the reservoir. This modification allowed for a robust calibration of the monitor data.

The calibration was performed in four steps. First, we matched the phase of the monitor data to that of the baseline survey by applying a 34 deg phase rotation, followed by a global time-shift of 7.28ms to better align reflections in time. Second, we applied a zero phase Wiener-Levinson least-squares filter to adjust the wavelet of the monitor to match the baseline in a least squares sense. Third, we calculated an applied trace-by-trace time-shifts to match the time structure of the Monitor Devonian event of that of the Baseline data. This pushed the anomalies of the monitor survey upward in time, altering the time structure of events within the reservoir and overlying strata. Finally, we scaled the amplitudes of the monitor data to match those of the baseline survey through a cross-normalization routine.

Overall, the calibration procedure effectively preserved all reservoir anomalies which are related to production, while minimizing or removing all other data differences which were not related to steam injection. Figure 12 is a comparison of an inline through the monitor volume to the same inline through the baseline data.

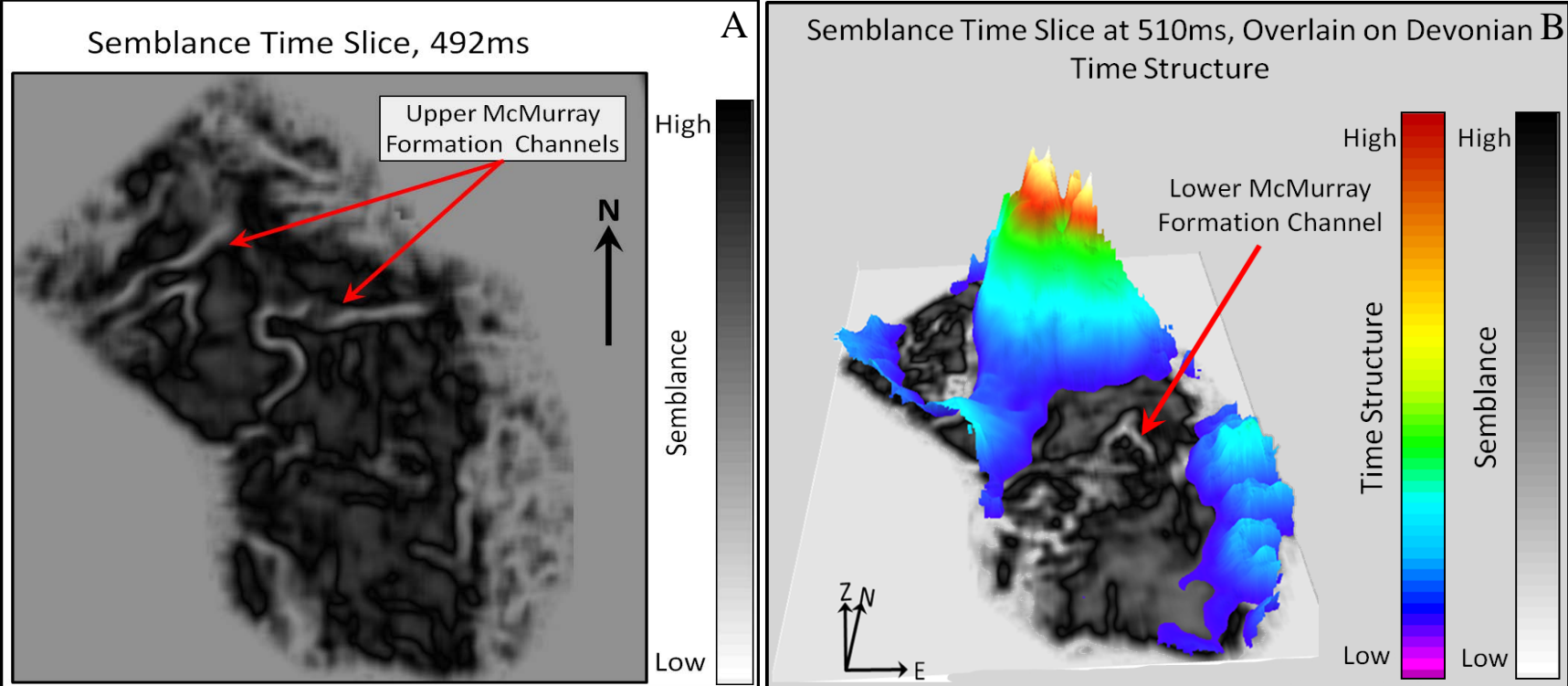


Figure 9 (a) Time slice at 492ms through the semblance volume, displaying channels within the Upper McMurray Formation. (b) Semblance time slice overlain on a 3D view of the Devonian time structure, displaying a McMurray Formation channel within a low along the Devonian surface.

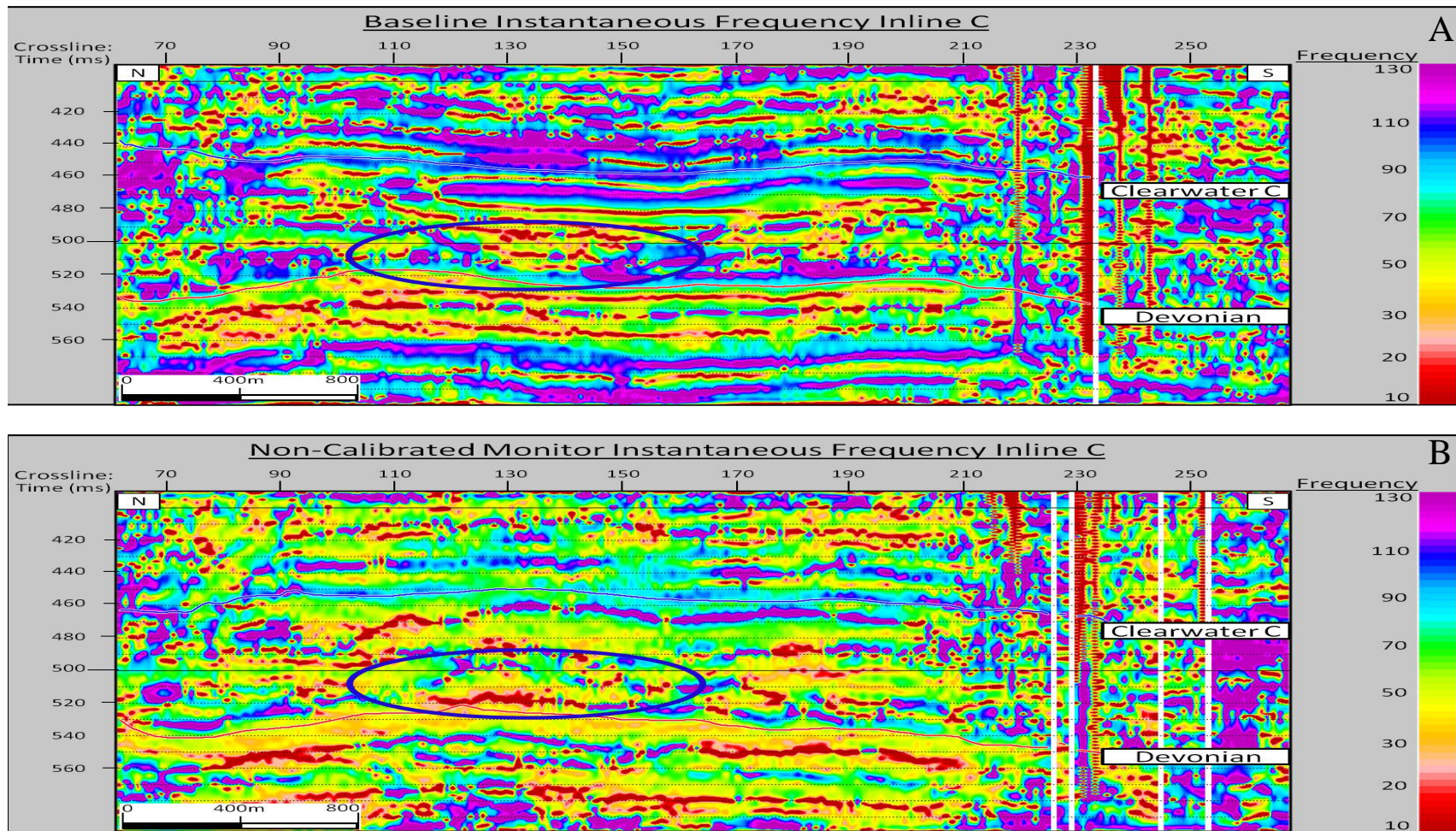


Figure 10 Inline C through the instantaneous frequency volumes for (a) baseline and (b) non-calibrated monitor displaying a lower frequency value on the monitor data than on the baseline data between crossline 110 and 150 at a time of 510 – 530 ms. The attenuation of high frequencies is attributed to steam injection. The red vertical lines represent errors in the frequency calculation due to gaps in the data.

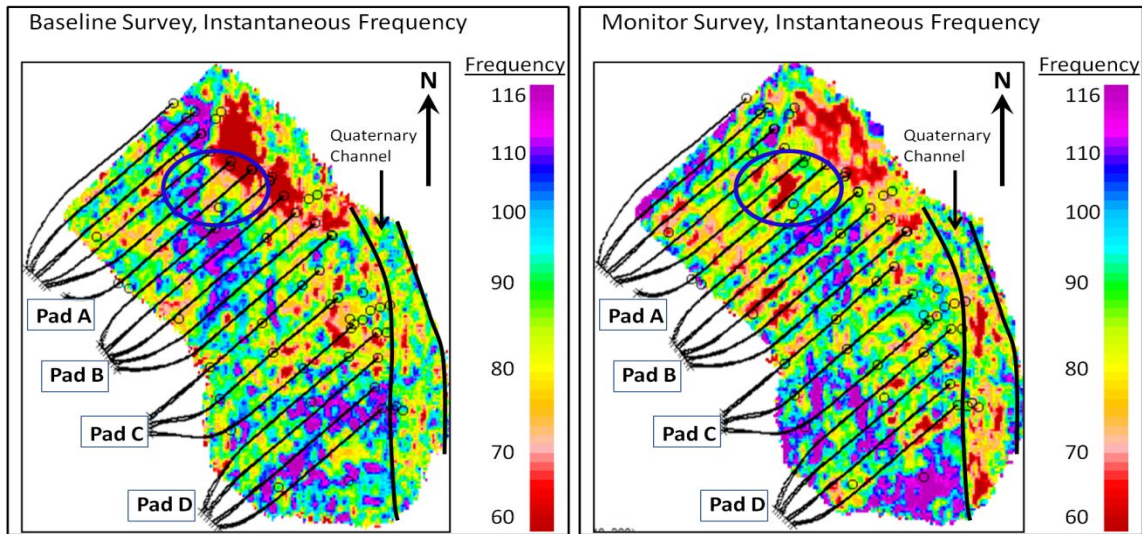


Figure 11 Instantaneous frequency slices calculated from 507 - 527ms for (a) baseline and (b) non-calibrated monitor displaying lower frequency values on the monitor survey than on the baseline survey, which correspond to horizontal well locations. The attenuation of high frequencies on the monitor survey is interpreted to be indicative of steam injection.

Figure 13 displays a crosscorrelation map for the caprock interval after data calibration. Due to the upward propagation of the reservoir anomalies, low correlation values are observed within the cap rock interval. Corresponding time-shift values reflect the low correlation regions (1.5 – 2.4 ms).

Figure 14 displays the crosscorrelation map for the McMurray Formation reservoir interval after data calibration. The delineation of the low correlation values have improved, reflecting the spatial location of the reservoir steam. Two zones of steam injection are clearly observable, in comparison to one from before calibration. Corresponding time-shift values are overall low (-1.0 to +1.0) with anomalously low regions reflecting the low correlation values.

The crosscorrelation values across the Devonian event are overall very high, ranging from 0.90 to 1.00, reflecting the effectiveness of the calibration process at matching the time-structure of the monitor Devonian event to that of the Baseline data. Overall time-shift values average 0ms. NRMS values for the Devonian event are significantly reduced, where overall NRMS values are 30 percent (Figure 16).

Difference Volume

After the calibration procedure, a difference volume was created, where the baseline survey data were subtracted from the monitor survey data. This difference volume removed all repeatable traces, leaving only the difference between the two surveys. The Devonian reflection is almost completely removed from the difference section due to the matching of the Devonian event between surveys in the calibration procedure. All reflection differences overlying the Devonian event will remain, as well as any amplitude anomalies that are due to the injection of steam within the McMurray reservoir. The

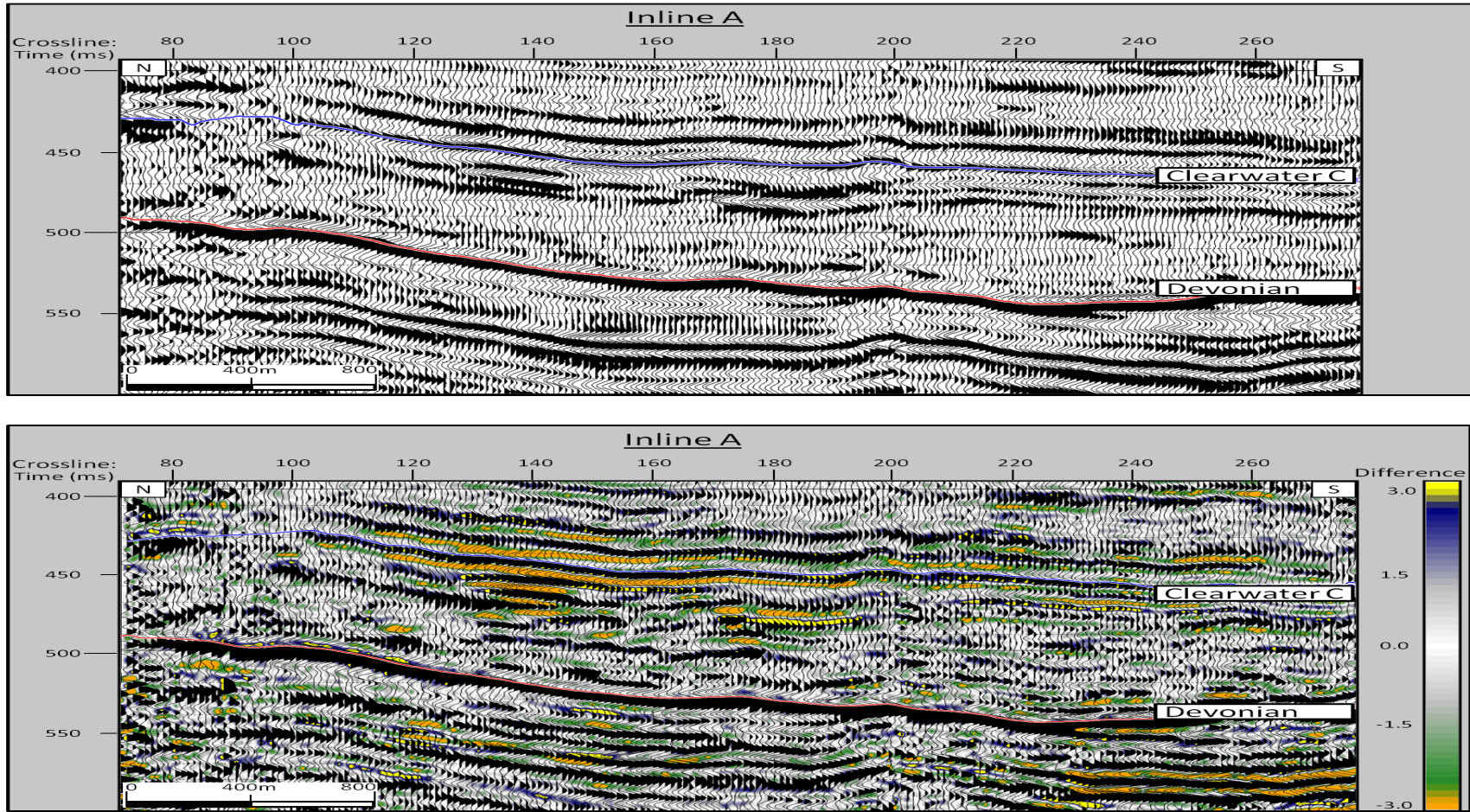


Figure 12 (a) Inline A through the baseline survey. (b) Inline A through the monitor survey after data calibration. The Devonian event of the monitor data now matches the Devonian event of the baseline due to the static corrections. Also, the caprock and overlying strata are largely similar, except for the time-delay difference that have been propagated upward through the calculation process. The color overlay is the amplitude difference between the baseline and monitor survey, calculated by subtracting the baseline data from the monitor data.

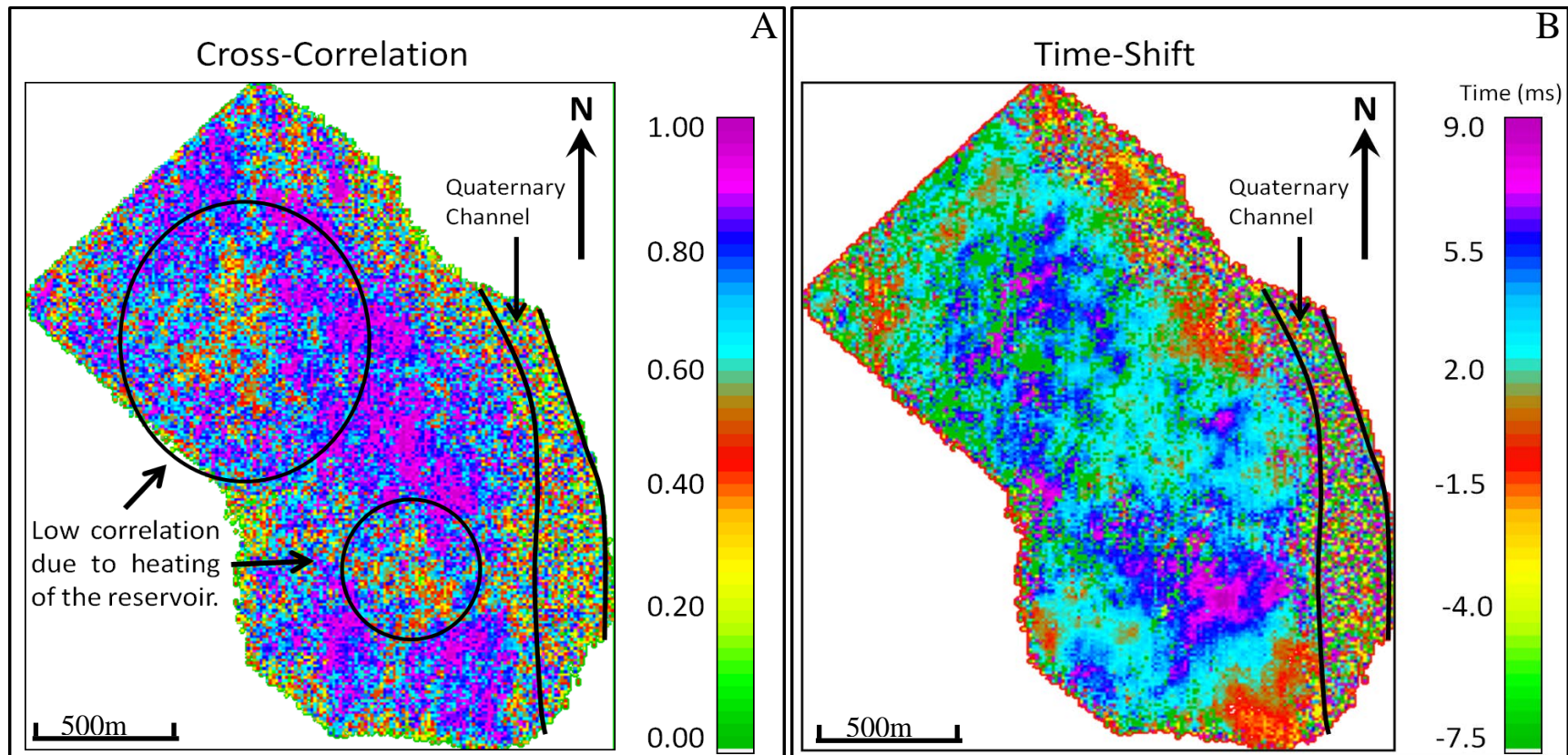


Figure 13 (a) Crosscorrelation map for the caprock interval, showing two areas of low crosscorrelation corresponding to the upward propagated reservoir anomalies through the static correction. (b) Corresponding time-shift values, displaying an overall low value of 0 – 2 ms. Two regions of high time-shift values are observed (7 – 9 ms), which correspond to low crosscorrelation values in (a). The combination of low correlation and high time-shift values is consistent with observations made within the McMurray Formation reservoir for steam induced anomalies (Figure 14).

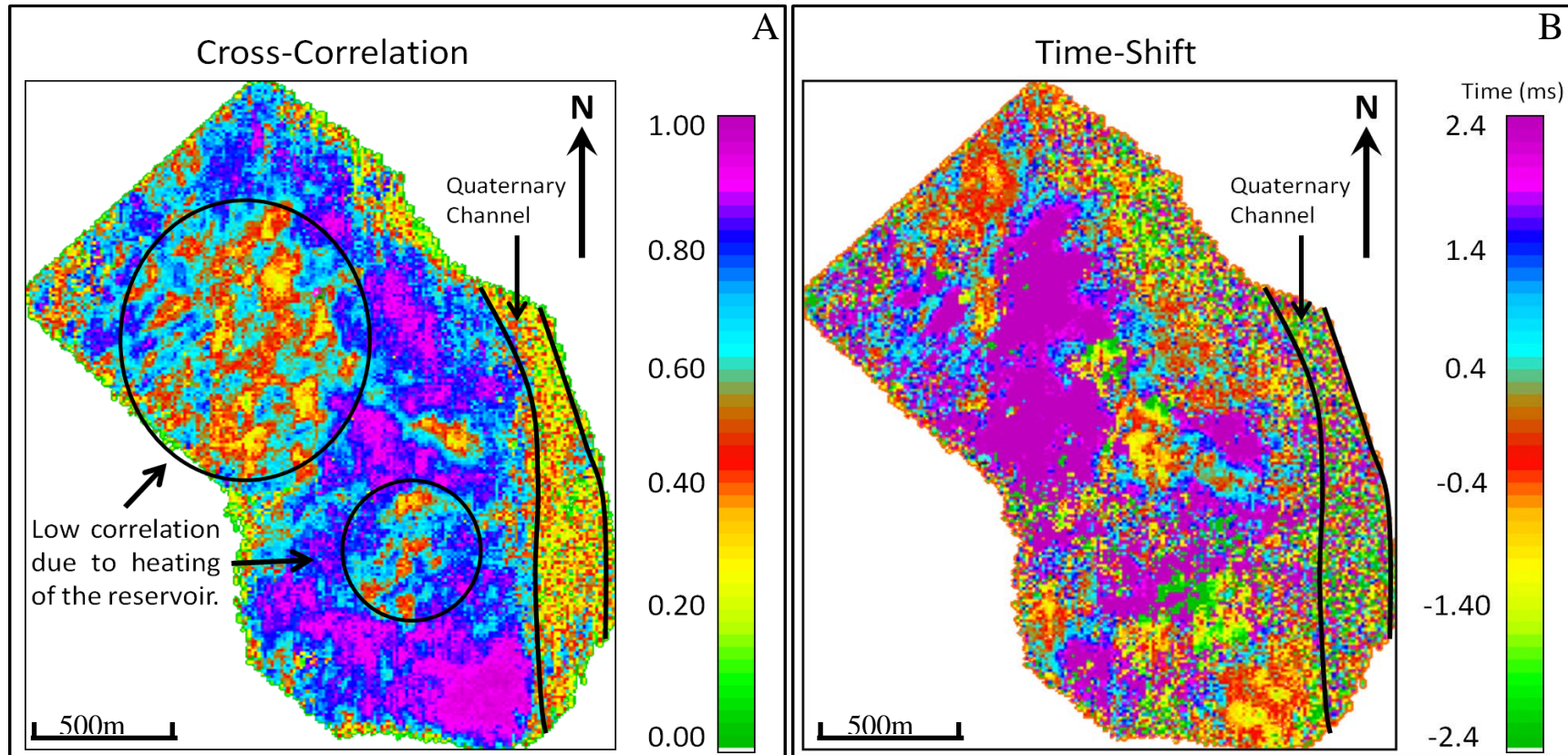


Figure 14 (a) Crosscorrelation map for the McMurray Formation reservoir interval after static correction displaying a low correlation value of 40-50 percent in areas of known steam injection and a high value of 80-100 percent areas not expected to have steam. The spatial definition of the low and high correlation values have improved in comparison to those before calibration (Figure 5). (b) Corresponding time-shift values for the McMurray Formation interval. High time-shift values of +2.0 to 2.4 ms coincide with low crosscorrelation values representing steam injection. Average time-shift values range from -1.0 to +1.0ms (excluding time-shifts for the steam zones).

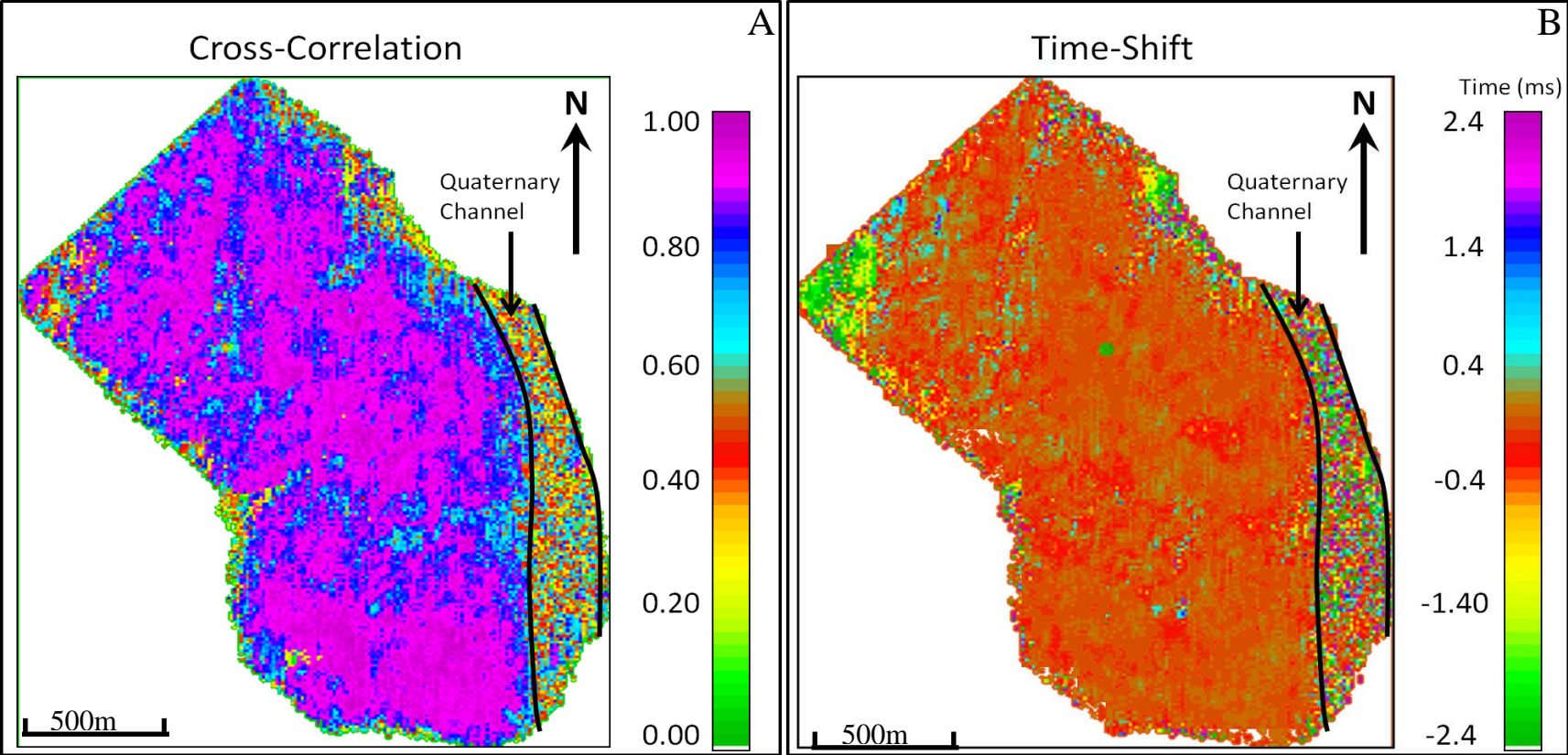


Figure 15 (a) Crosscorrelation map for the Devonian interval after data calibrations showing a high overall correlation between the baseline and calibrated monitor data between 90 - 100%. In comparison to before calibration (Figure 4), values are significantly increased. The time-shift map (b) for the Devonian interval displays a time-shift values of 0 ms for the corresponding crosscorrelation values of 90 to 100 percent, a significant increase over the time-shift values before the calibration.

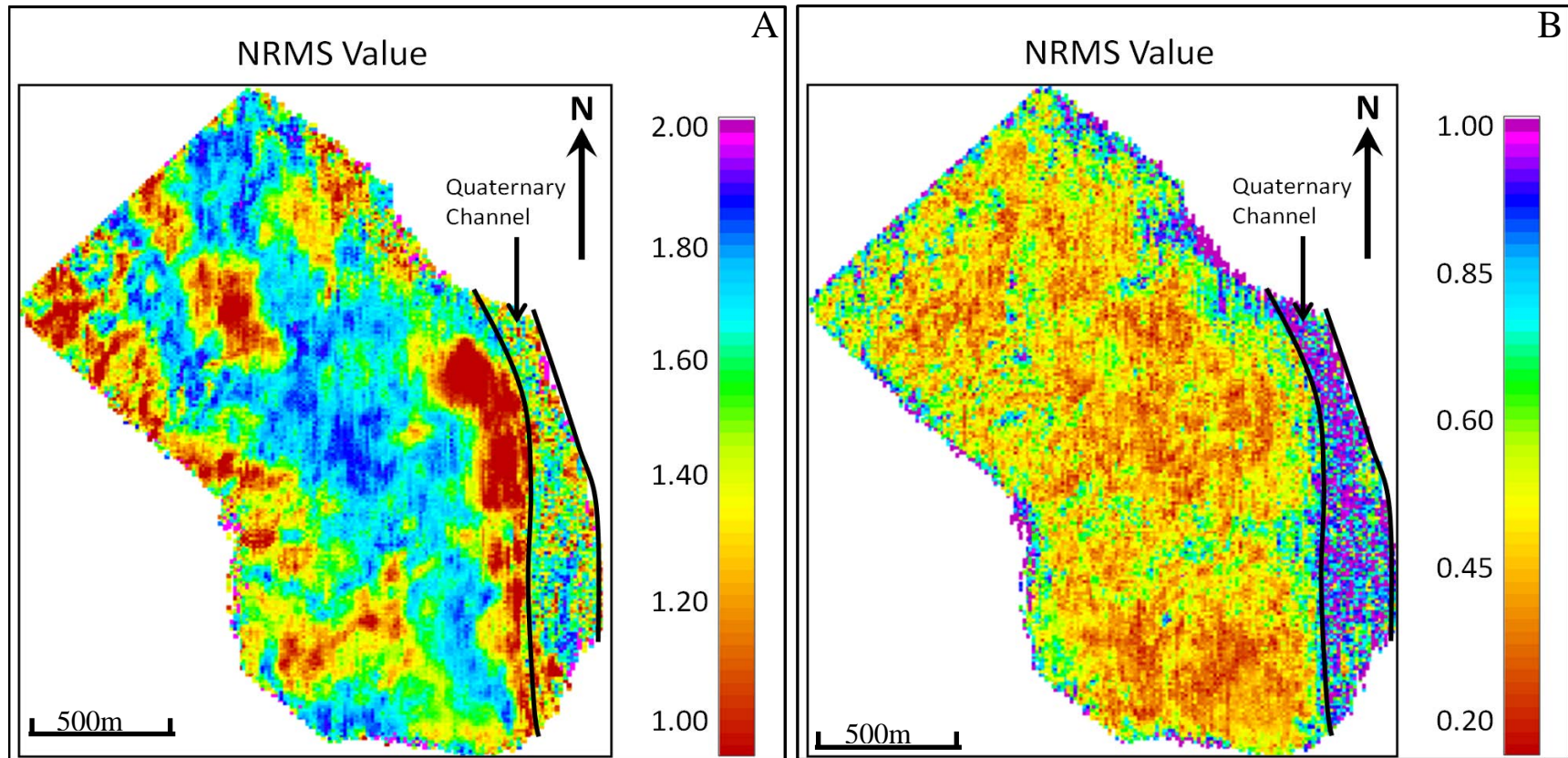


Figure 16 A comparison of (a) NRMS values across the Devonian event before calibration and (b) NRMS values across the Devonian event after data calibration. The final NRMS values are consistent across the entire survey area (except for the Quaternary channel region) and display values as low as 18 – 20 percent, with an average NRMS value of 30percent. In comparison, average NRMS values prior to calibration were 140.

difference volume was flattened along the Clearwater C event to aid in interpretation. The two volumes will be referred to as (1) the difference volume and (2) the flattened difference volume throughout the remainder of this chapter.

Figure 17 is an inline section through the flattened difference volume. From 470-500 ms, between crosslines 160 to 200, we observe a large amplitude anomaly, possibly representing a steam chamber. Taking a time slice through the flattened difference volume at 485 ms, and overlaying the horizontal well pairs, we observe that the amplitude anomaly corresponds with the injection wells of pads B and C (Figure 18). Thus, we interpreted this amplitude anomaly to be related to steam injection. A second anomaly is observed between crosslines 120 – 140 at a time of 460ms. Again, the time-slice displays the correlation of the anomaly with the horizontal well pairs, supporting the interpretation that the anomalies are due to steam injection into the McMurray Formation reservoir.

Observed amplitude anomalies within the difference volume appear to be located within the upper McMurray Formation, but are observed at later times on the monitor data prior to calibration. Following the global and trace-by-trace time shifts applied during calibration, the amplitude anomalies have been propagated to earlier times, and hence will be observed in the upper McMurray Formation on the difference volumes despite their original positioning within the Lower McMurray Formation on the non-calibrated monitor data (see section 4.4 and section 4.5).

Data Calibration Discussion

NRMS, crosscorrelation and time-shift maps were used to understand the effectiveness of the calibration procedure, and for quality control purposes. Each step in the calibration process employed these tools before and after the application of a correction to ensure the accuracy and effectiveness of each process. Every correction increased crosscorrelation values and reduced time-shift and NRMS values calculated across the Devonian reflection.

Following calibration, crosscorrelation maps within the reservoir exhibited high values in areas without steam injection, and low values in areas where steam has created anomalies on the monitor survey. Corresponding time-shifts have been reduced to negligible values. Crosscorrelation values through the caprock interval displayed low values in regions where reservoir sourced anomalies were propagated to earlier times through the calibration procedure, and high values in areas free of reservoir induced anomalies.

The NRMS maps were significantly altered by the calibration procedure, where NRMS values were dependent upon the phase, static and amplitude difference between the two datasets (Sheriff, 2002; Kragh & Cristie, 2002). After these differences were corrected, NRMS maps exhibited low overall values across the Devonian interface of 20 percent (Figure 16).

Calibrating the data using the Devonian reflection propagated the time-lapse anomalies to earlier times instead of later times, thus moving reservoir difference into the upper McMurray Formation, the Clearwater Formation and the overlying strata. Hence,

reservoir anomalies were observed on difference volumes within the Upper McMurray Formation and overlying caprock and strata (Figure 12).

Due to the calibration procedure, time delays were removed from the Devonian reflection, shifted earlier in time through static corrections. These propagated time delays are observable in the cap rock region of the difference volume, where high amplitude, laterally continuous events are observed above the steam induced amplitude anomalies (Figure 17). These cap rock anomalies are created by subtracting the flat cap rock reflections of the baseline data from the reflection from the calibrated monitor survey that are no longer flat due to propagation of the time delays earlier in time. Hence, these anomalies represent heating of the reservoir, where elevated reservoir temperatures have reduced the velocity of P-waves traveling through the reservoir (Nur, 1982; Wang & Nur, 1988; Eastwood, et al., 1994). Reservoir temperature levels are elevated beyond the extent of the steam chambers, thus, time delays are observed to coincide with amplitude anomalies, but extend further than the lateral extent of the steam. Hence, anomalies in the cap rock region are more laterally continuous than the amplitude anomalies within the reservoir, and reflect heat distribution.

TIME-LAPSE INTERPRETATION

The time-lapse interpretation was focused on the identification of travel time shifts and amplitude anomalies within the reservoir, primarily observed within the difference volume. The observation of a significant time delay, coupled with an amplitude anomaly within the reservoir and the correlation to horizontal SAGD wells comprised the bulk of the P-wave time-lapse interpretation.

Other techniques were employed to further support the observation and interpretation of amplitude anomalies within the reservoir, including isochron analysis, amplitude anomaly distribution mapping, an instantaneous amplitude volume, and the integration of well log data.

Isochron Analysis

Isochron maps display time variations between two seismic events. Effectively, they can be thought of as time thickness maps, displaying the variation in travelttime between two events (Eastwood, et al., 1994; Isaac, 1996). Isochron maps are a quick and effective technique for identifying areas of increasing or decreasing travelttime between a baseline and monitor survey. Because the reservoir thickness did not change over time, differences in isochron maps between the baseline and monitor data are representative of P-wave velocity decrease in the monitor data (Nakayama, et al., 2008). Isochrons were built over the reservoir interval, bounded by the Devonian horizon and the Clearwater C horizon on both the baseline and calibrated monitor data. Figure 19 is a comparison of the baseline and monitor isochron maps. There is significant travel time thickening in areas of steam injection, due to the travelttime delay created by the lower velocity of heated bitumen. As discussed in Chapter 1 (section 1.3), the injection of steam into bitumen saturated reservoir

reduces P-wave velocity up to 30 percent (Wang & Nur, 1988; Eastwood, 1993). A velocity reduction will create time thickening within the reservoir, represented as an increase in isochron thickness in a time-lapse sense. Taking the difference of two isochrons accentuates the time delays (Figure 21)

It is important to consider that the decrease in velocity signifies heating of the reservoir and not solely the presence of steam. The reservoir can be heated at a distance greater than that of the steam distribution. Thus, there are portions of the reservoir which do not contain steam but have elevated temperatures, creating a traveltime increase. Consequently, the isochron difference map is representative of the heat distribution and not of steam distribution.

Amplitude Anomalies

The flattened difference volume was analyzed for the presence of amplitude anomalies within the McMurray Formation reservoir. Figure 18 shows an inline through the center of the difference volume displaying two anomalies interpreted to be due to the injection of steam into the reservoir, with overlying anomalies in the cap rock due to heating induced time delays. Figure 22 is a chair cut display of the flattened difference volume, combined with an intersecting inline and crossline, displaying time delay anomalies within the cap rock interval, as well as steam amplitude anomalies within the McMurray Formation reservoir. As previously discussed, anomalies due to time delays were observed within the caprock interval, while anomalies due to steam injection were observed within the McMurray Formation reservoir.

Reservoir amplitude anomalies were observed throughout the difference volume and largely correspond with locations of horizontal wells and also with isochron time delays (Figures 18, 20). This identification procedure was employed throughout the flattened difference volume, yielding multiple observations of amplitude anomalies within the McMurray reservoir.

To garnish our understanding of the distribution of amplitude anomalies throughout the entire reservoir, we adopted a technique developed by McGillivray (2005) for identifying the spatial distribution of heat within a reservoir. Using the flattened difference volume, the positive amplitudes were analyzed throughout the McMurray Formation reservoir. The reservoir interval was defined as the time interval 5ms lower than the flattened Clearwater C horizon to the Devonian horizon. The addition of 5 ms to the Clearwater C horizon ensured that the calculation of the amplitude anomalies did not include the anomalies present within the cap rock interval. Amplitude values were analyzed on a slice-by-slice basis, summed and displayed in map view, yielding the total distribution of the positive amplitude anomalies within the reservoir. This technique was also applied to the largest negative amplitude anomalies. Figure 23 is a map view of the positive and negative amplitude distributions. There are two large amplitude anomalies in the study area, one in the north corresponding to pads A and B and one in the south corresponding to pads C and D. Overlaying the well pairs onto the anomaly distribution maps highlights the correspondence of well placements with amplitude anomalies.

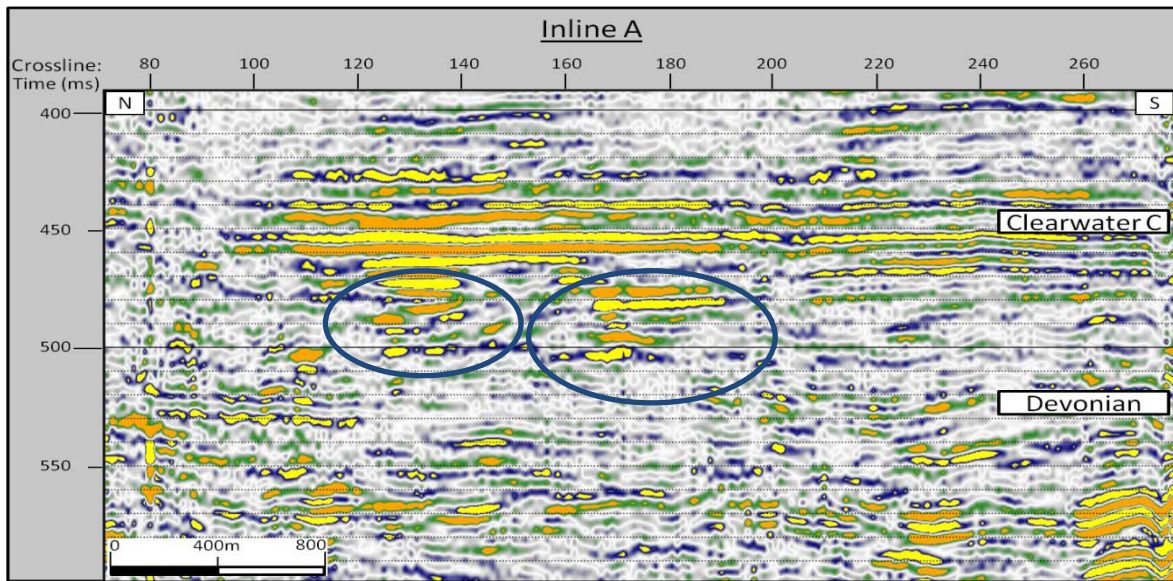


Figure 18 In-line A through the flattened difference volume. The two highlighted ellipses represent large amplitude anomalies within the McMurray reservoir due to steam injection. The laterally continuous anomalies overlying the steam anomalies are created from time delays due to heating, propagated upward into the cap rock reflections during the calibration procedure.

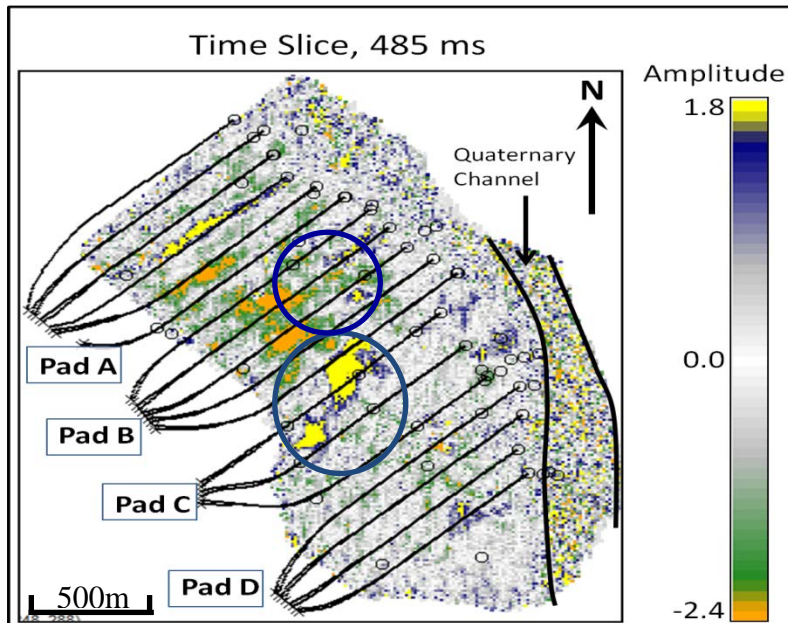


Figure 19 Time slice through the flattened difference volume at 485ms displaying amplitude anomalies and their correlation with horizontal well pairs. The circles represents the anomalies observed in Figure 4-18.

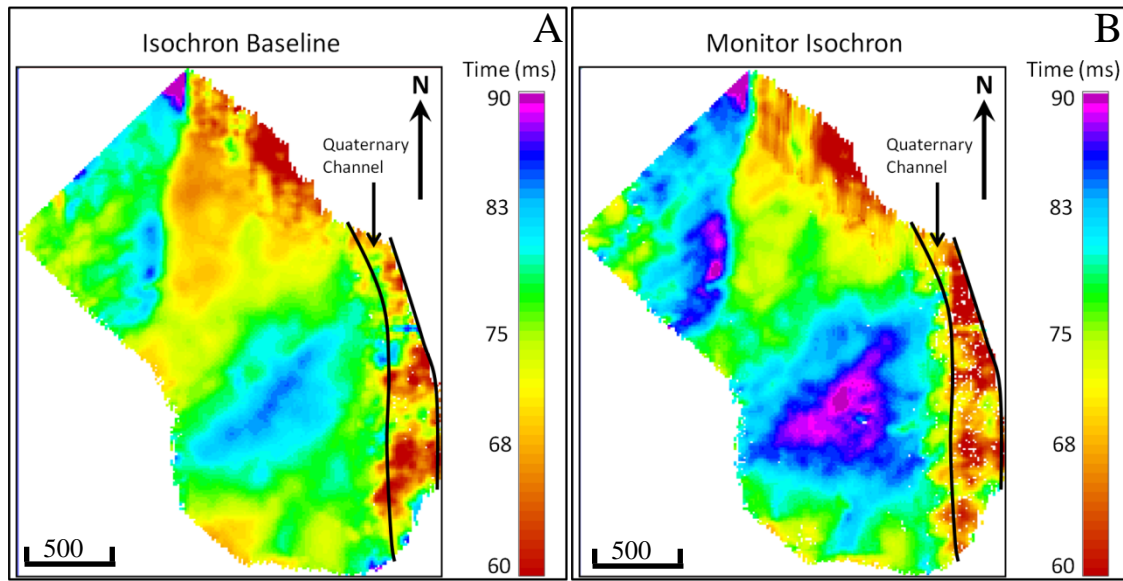


Figure 20 A comparison of (a) baseline isochron and (b) monitor isochron. Significant time delays are observable on the monitor isochron due to heating within the McMurray Formation reservoir.

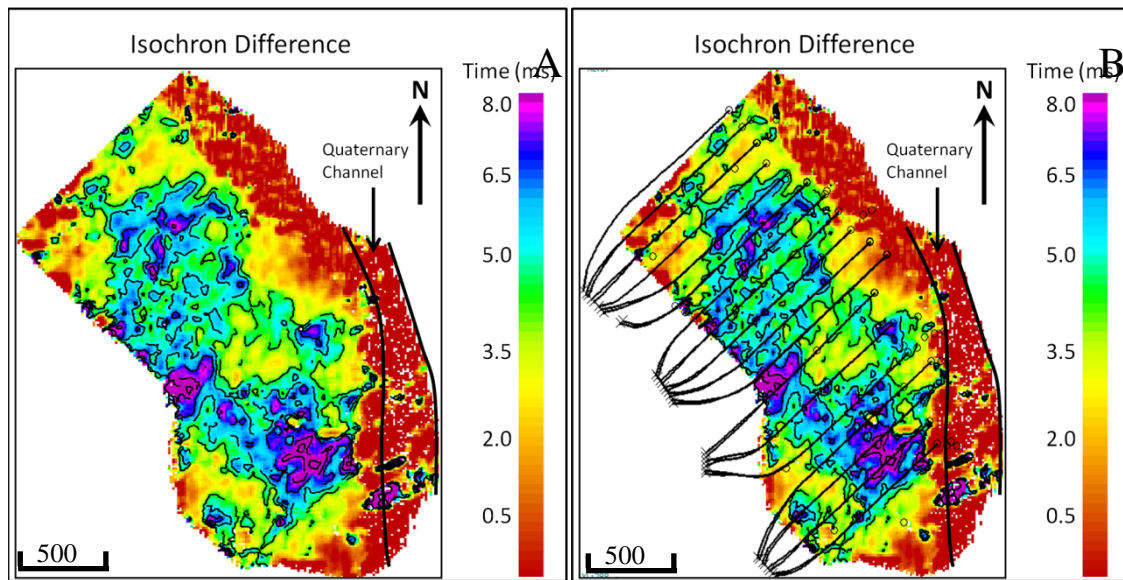


Figure 21 (a) Isochron difference map and (b) Difference map with horizontal wells overlain on time delays, highlighting their relationship. Contours highlight time delay difference between the baseline and monitor survey. Contours range from 4.0 ms to 8.0 ms in increments of 1.0 ms.

The anomalies on both the positive and negative distribution maps appear to follow the paths of the horizontal wells. From this, I interpret that the amplitude anomalies contained within the McMurray reservoir interval are likely a result of steam injection and thus are representing the reservoir heat and steam distribution in a spatial display.

The observed amplitude anomaly distributions coincide with areas of increased traveltime. Figure 24 is a comparison of the isochron difference map to the positive amplitude anomaly distribution map. A strong correlation between traveltime delays and amplitude anomalies were observed, thus supporting the interpretation that the increase in traveltime within the McMurray Formation reservoir on the monitor survey is a result of reservoir heating, creating a time delay for waves propagating through the reservoir. However, the distribution of time-delays is greater than that of the amplitude anomalies. Reservoir temperatures levels are elevated beyond the extent of a steam chamber, creating time delays that are not associated with amplitude anomalies within the McMurray Formation reservoir (as discussed in section 4.5.6). Thus, the isochron distribution map is representing the distribution of heat within the McMurray Formation reservoir, while the amplitude anomaly distribution map is representative of steam-induced anomalies (the amplitude anomaly distribution maps did not include the amplitude anomalies of the cap rock region that were created from the calibration procedure; section 4.5.6).

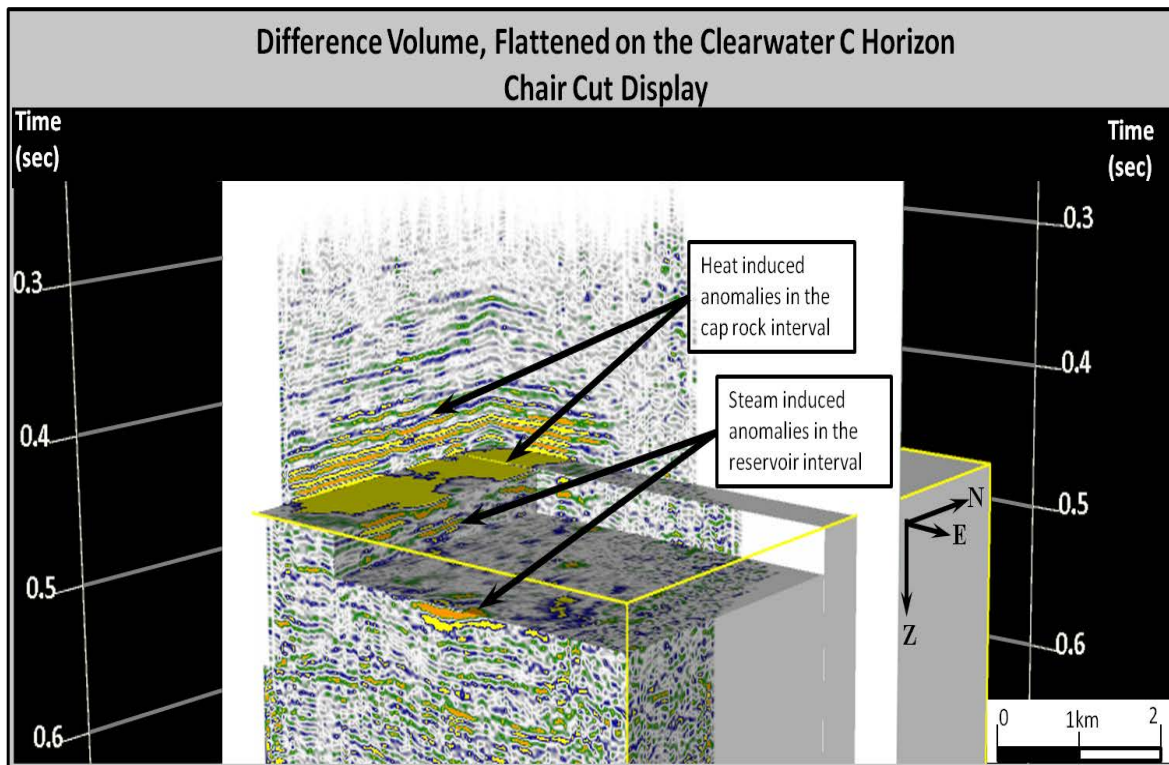


Figure 22 Chair-cut display of the flattened difference volume, combined with an intersecting inline and crossline. Amplitude difference anomalies are observed within the caprock interval, due to heating induced time delays, as well as within the reservoir due to steam.

Northern Anomaly

A further point of interest is the asymmetry of the heat distribution. Although the amplitude anomalies tend to follow the horizontal well paths, the anomaly in the north also contains a northern trend, perpendicular to well orientation. The flow pathway of the heat appears to be between injection wells, connecting the well pairs of pad B to those of

pad A. Pads A and B produced approximately 3.61 million barrels of oil from February 2008 to January 2011, the latter being the time of recording of the monitor survey.

Figure 26a is a well log cross section running SW-NE along the northern amplitude anomaly. There is a very large succession of channel sands observable from the gamma ray logs, through which heat may flow from the wells of pad B and connect to the wells of pad A to the north.

The amplitude anomaly terminates along a NNE trend prior to the toe end of the wells, interpreted to indicate the intersection of a muddy or silty unit and inefficient steam distribution. An East-West cross-section along wells B, C and D displays a thick channel sand, bounded to the East and West by a large mud interval (Figure 26).

The boundaries of the amplitude anomaly correlate with the channel boundaries observed within the semblance volume (Figure 9) Figure 27 displays the positive amplitude anomaly distribution map overlain onto the semblance time slice at 492ms. The edges of the steam distribution show a strong correlation with the channel boundaries. This correlation is interpreted to be representative of steam within a large sand-filled channel, which is bound to the east, west and northwest by muddy HIS bedding, restricting steam growth outside of the sand-filled channel. The semblance is displaying the edges of the sand filled channel.

Southern Anomaly

The southern anomaly is interpreted to show a more symmetrical heat distribution, flowing between the wells in pads C and D. This anomaly is more localized than its northern counterpart, where a significantly large area along the heel of pads C and D does not show any heating. Figure 26 is a well cross section through the southern anomaly. Well E intersects the horizontal wells of pad D, and displays a large succession of channel sands with an elevated reservoir temperature of 80 degrees Celsius. Well F to the west intersects the heel of the same horizontal well, outside of the heat anomaly, and displays a mud or shale unit structurally equivalent with the heated sands of well E. This mud may be a baffle to steam flow, currently preventing the heat from reaching the overlying channel sands. The reservoir temperature recorded in well E (80 deg C) is relatively low considering the long period of injection (November 2007- January 2011) and the higher temperatures observed in other temperature logs of 200 deg C and above. This low temperature suggests that there may be a nearby thief zone, which would steal injected heat and steam from the reservoir along the horizontal wells of Pad D.

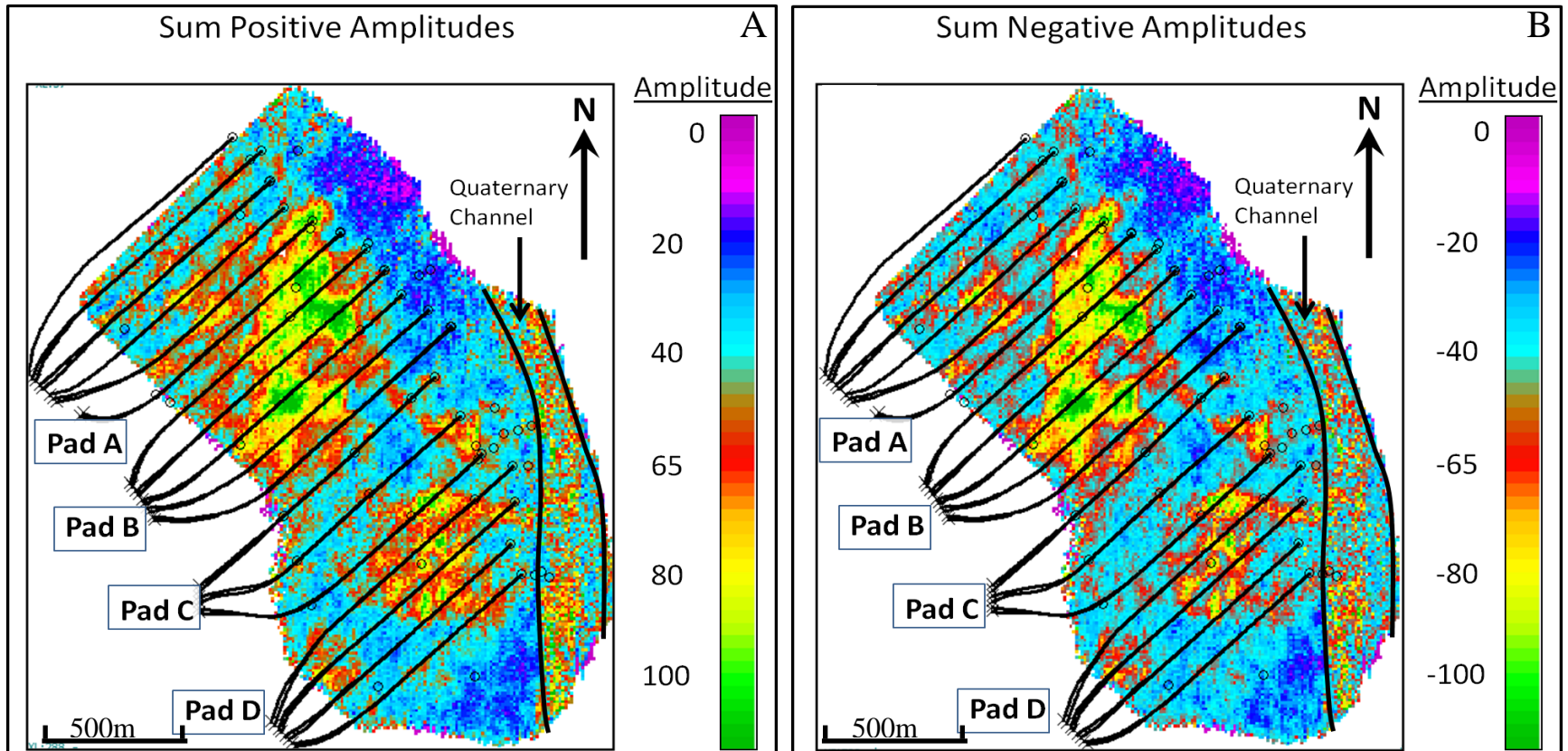


Figure 23 Amplitude anomaly distribution within the McMurray Formation reservoir for (a) Sum of positive amplitudes and (b) Sum of negative amplitudes. A northern and a southern anomaly are observed, representing heat distribution within the reservoir.

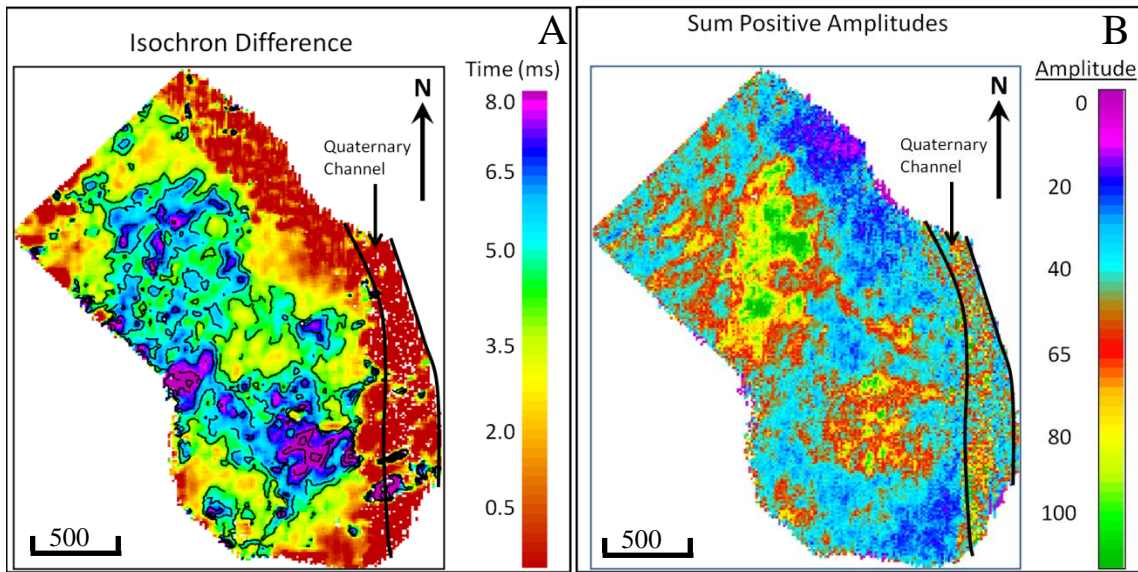


Figure 24 Comparison of (a) isochron difference map to (b) amplitude anomaly distribution map. Regions of high traveltimes correlate with amplitude anomaly distributions. However, the time-delay distribution is larger than the amplitude anomaly distribution, suggesting the time-delay map is representative of heat distribution, while the amplitude anomaly map is representative of steam distribution.

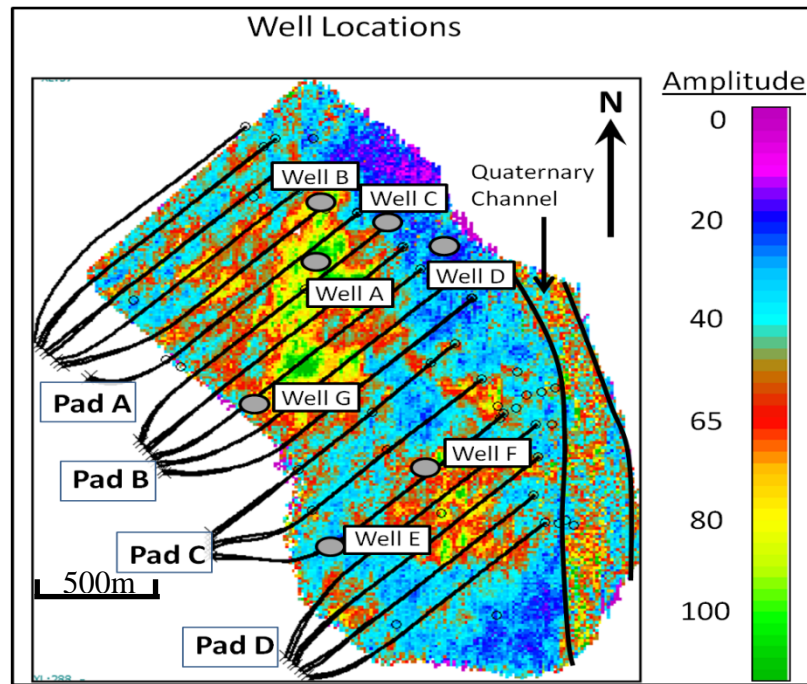


Figure 25 Amplitude anomaly map displaying the locations of wells A – G used in the well log cross sections, Figure 4-34.

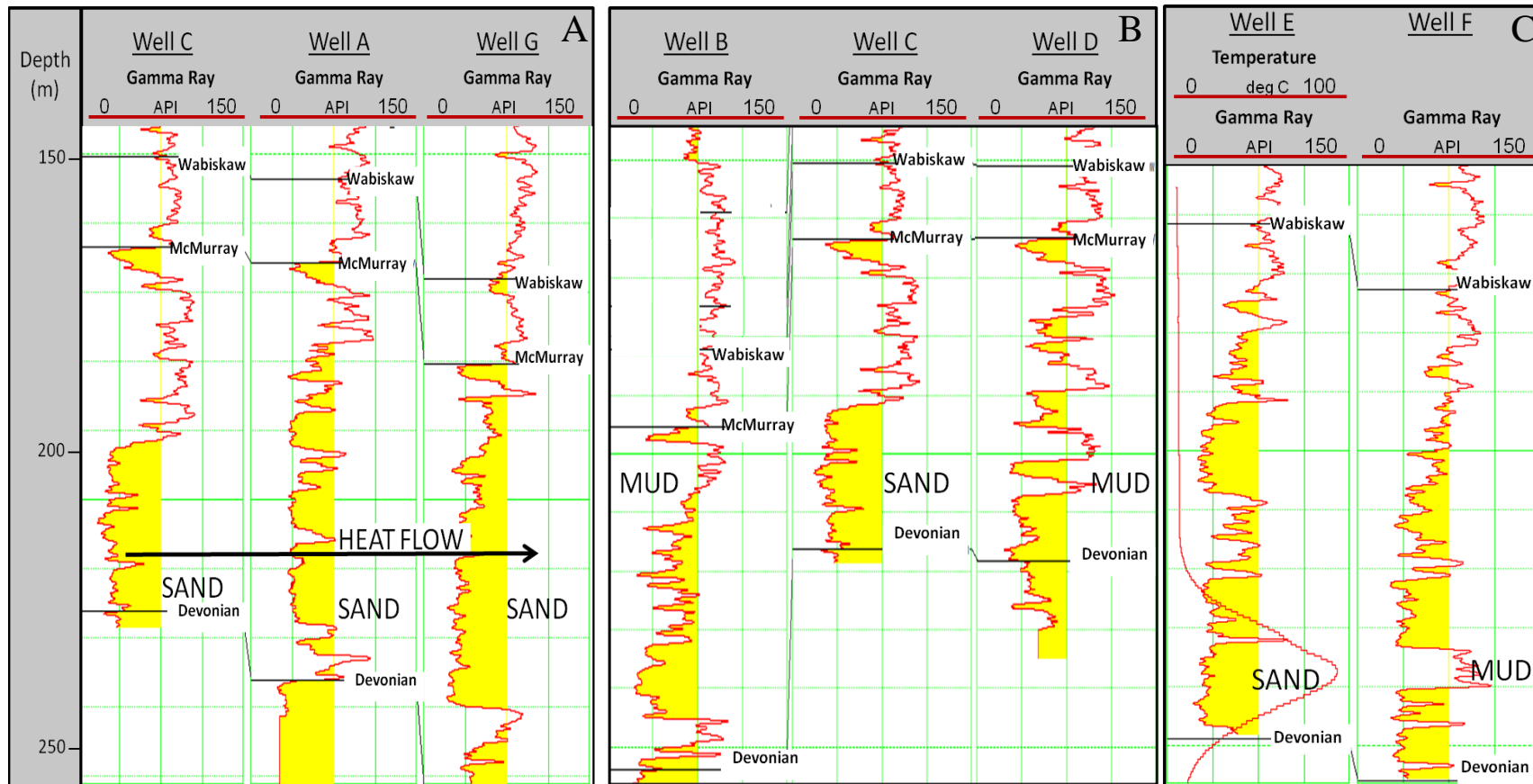


Figure 26 Well log cross section constructed using Gamma Ray logs. (a) Cross section through the northern anomaly displaying structurally equivalent channel sands, interpreted to be allowing heat flow between the horizontal wells of pads A and B (b) Cross section through the northern anomaly displaying a large channel sand juxtaposing two muddy intervals to the east and west (c) Cross section through the southern anomaly displaying a heated channel sand structurally equivalent to a thick mud. A temperature log is overlain on the gamma ray log, displaying elevated reservoir values within the McMurray Formation reservoir. Logs are recorded in depth as measured from the Kelly bushing, displaying the structural features of the McMurray Formation reservoir.

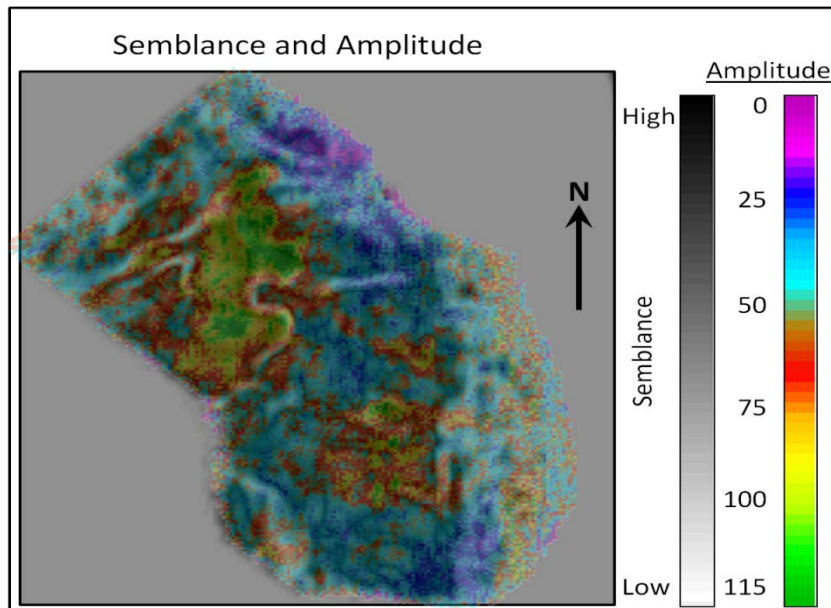


Figure 27 Sum of positive amplitudes (transparency 70%) overlain on semblance time slice at 492ms, displaying the correlation of northern amplitude anomalies with channel edges. Low semblance values are interpreted to be channel edges (

Pads C produced approximately 1.68 million barrels of oil from May of 2003 through to January 2011 and pad D produced approximately 2.70 million barrels of oil from November of 2007 to January of 2011 for a total of approximately 4.38 million barrels of oil.

Instantaneous Amplitude and Instantaneous Phase

To provide further support for the distribution of heat within the reservoir, complex seismic trace analysis was employed to generate an instantaneous amplitude volume. The instantaneous amplitude (also known as amplitude envelope or reflection strength) is a measure of the total energy of a signal, or the maximum value of the seismic trace under a constant phase rotation (Schmitt, 1999; Barnes, 2007). Instantaneous phase is the phase angle required to rotate a seismic trace to its maximum value (Barnes, 2007). Thus, a seismic trace can be represented as a product of two independent functions, instantaneous amplitude and instantaneous phase. These two functions separate the phase and amplitude information in seismic data, and are the fundamental seismic attributes used to derive all other attributes (Barnes, 2007).

Instantaneous amplitude calculations are a measure of reflection strength, independent of polarity or phase of a reflection. Thus, its maximum value may be different from that of the largest peak or trough of a reflection (Taner, et al., 1979; Sheriff, 2002; Barnes, 2007). High amplitude envelope values are associated with abrupt lithological changes, gas accumulations, or in the case of SAGD, steam injection. Instantaneous amplitude is defined as follows (Tanner, 2002; Barnes, 2007):

$$a(t) = \sqrt{x^2(t) + y^2(t)} \quad 6$$

where $x(t)$ is the seismic trace and $y(t)$ is the seismic trace rotated by -90 deg, which is the Hilbert transformed trace. The phase rotation angel (angle required to rotate the trace to its maximum) is defined as (Tanner, 2002; Barnes, 2007):

$$\theta(t) = \arctan \left[\frac{y(t)}{x(t)} \right] \quad 7$$

Instantaneous phase is a representation of the seismic data with the amplitude information removed. Its values represent the apparent position along a cosinusoid such that peaks have a 0 deg phase and troughs have 180 deg phase (Barnes, 2007).

Instantaneous phase and instantaneous amplitude have been employed in seismic interpretation to aid in the identification of features of interest. Schmidt (1990) used instantaneous amplitude to define porosity zones within the Casper Creek Field. Hein et al. (2010) used instantaneous amplitude and instantaneous phase to identify bottom simulating reflectors of gas hydrates in the Ullung Basin. Riedel et al. (2011) used instantaneous amplitude to map gas hydrates within channel-levee systems in the Krishna-Godavari Basin. For this study, Instantaneous amplitude was found to be more effective than instantaneous phase for enhancing the visibility of the amplitude anomalies within the reservoir.

Figure 28 is an inline section through the calibrated monitor survey before and after the calculation of the instantaneous amplitude volume. There are large amplitude anomalies observed on the flattened difference volume, representative of steam injection into the McMurray reservoir. Through the transformation to the instantaneous amplitude volume, the phase content of the signal is removed, displaying a phase independent representation of the reservoir anomaly, characterized by positive amplitude values. The instantaneous amplitude volume enhances the representation of the anomalies within the section, and suppresses the visibility of noise.

Applying the positive amplitude analysis technique (section 4.7.1) to the instantaneous amplitude volume produced new heat distribution maps which account for both the positive and negative amplitudes of each event, represented as a single positive envelope value. Figure 29 is the map view distribution of heat generated from the positive amplitude analysis technique. It correlates very well with the previous heat distribution maps (Figure 23), however displaying a larger heat distribution due to its representation of the positive and negative values as positive values.

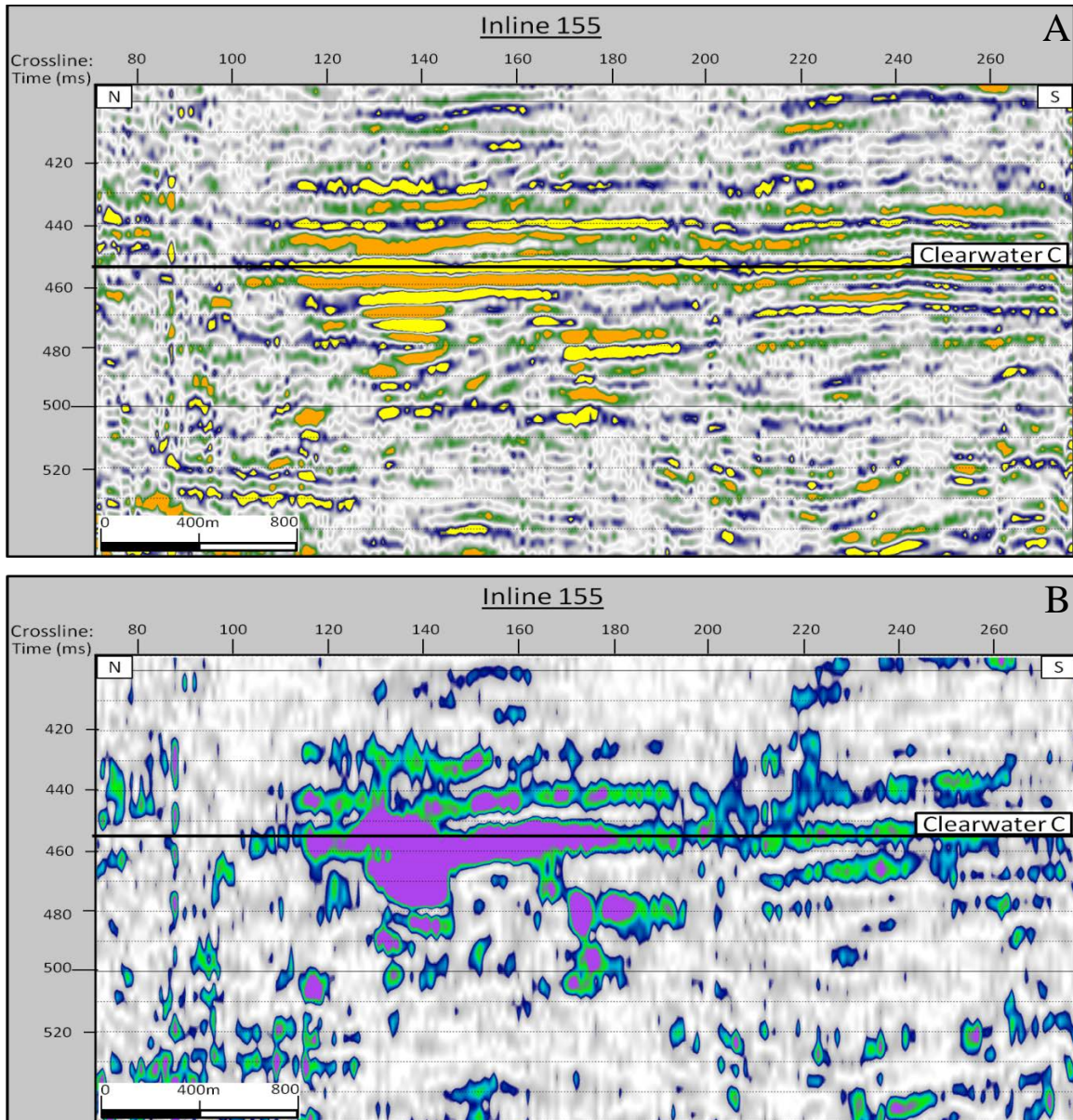


Figure 28 (a) Inline A through the flattened difference volume. The highlighted ellipse represents large amplitude anomalies within the McMurray Formation reservoir due to steam injection (b) Inline A through the instantaneous amplitude volume. The instantaneous amplitude representation of the amplitude anomaly is independent of phase, representing the peaks and troughs as a single positive amplitude value.

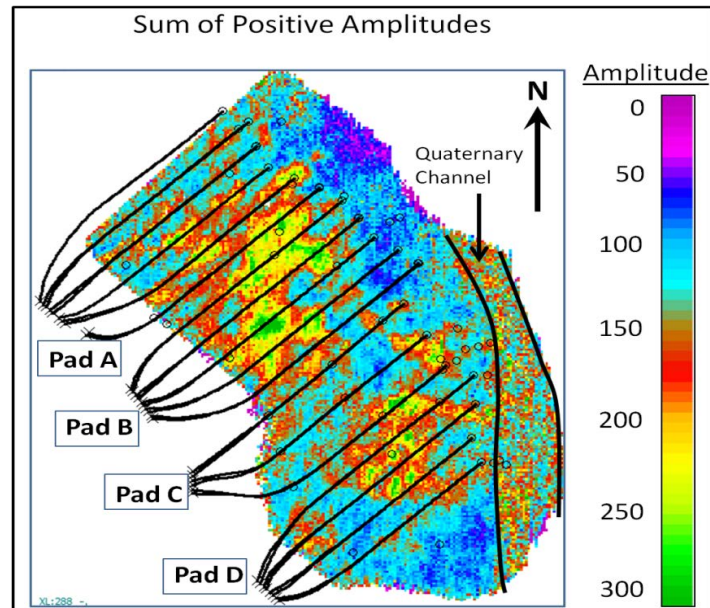


Figure 29 Sum of positive values through the McMurray reservoir, calculated on the amplitude envelope volume. The representation of the anomalies is free of phase, thus displaying peaks and troughs as a single positive amplitude value.

DISCUSSION

Taking advantage of the strong contrast between the baseline survey and a production influenced monitor survey, a detailed interpretation of reservoir changes over time was carried out. Preliminary interpretation of the baseline and monitor survey identified seismic horizons of interest with the aid of synthetic seismograms and well ties, identifying the temporal location of the McMurray Formation reservoir.

Amplitude anomalies were observed within Lower McMurray Formation, which overlaid time delays and zones of frequency attenuation on the Devonian reflection. Lower and Upper McMurray Formation channels were identified within the data on semblance time slices.

NRMS and crosscorrelation maps were constructed, identifying differences between the baseline and monitor survey which were related to phase, amplitude, and time differences. These differences were corrected for through the detailed calibration of the monitor data to the baseline data.

Following the calibration, difference volumes were constructed to aid in the interpretation of observed amplitude anomalies. Amplitude anomalies were identified throughout the McMurray reservoir in conjunction with velocity anomalies within the caprock (upward propagated from the Devonian after calibration).

McMurray reservoir isochrons were built using the baseline and calibrated monitor surveys to provide a quick view of time thickening within the reservoir. The reduction in

seismic velocity of the heated bitumen created significant traveltime delays, resulting in velocity pushdowns, identifiable as travel time increases on the reservoir isochrons. Taking the difference between the two isochrons accentuated these time delays, which correlate strongly with observed amplitude anomalies.

Amplitude anomalies were projected into map view, providing an examination of steam distribution within the McMurray reservoir, which was contained within two main regions. Correlating these distribution maps with the SAGD injection and production well pairs provided strong support for the relationship of observed amplitude anomalies to steam injection. These maps provided a projected spatial distribution of steam within the McMurray reservoir, as well as some information regarding heat flow, and steam connectivity between well pairs.

The amplitude anomaly distribution maps correlated well with the isochron difference map. However, difference between the amplitude anomaly maps and the isochron difference maps were observed, as displayed in Figure 24. It was interpreted that the isochron difference map is representing the distribution of heat induced time delays within the McMurray Formation reservoir, while the amplitude anomaly distribution map is representing the distribution of steam anomalies within the McMurray Formation reservoir.

Combining the amplitude anomaly analysis technique with the instantaneous amplitude volume provided further support for the interpretation of steam distribution within the McMurray reservoir. Correlating this data with the horizontal well pair locations supported the interpretation that the observed amplitude anomalies on both the difference volumes and the calibrated monitor volume are a result of the injection of high volumes of steam into the McMurray reservoir.

Integrating the geological interpretations provided from the well log cross sections to the geophysical observations, we interpret that the majority of the heat anomalies are located dominantly within two large McMurray channels which host the bulk of the McMurray sand (Figure 30). These two large channels trend towards the northeast, and are each comprised of a succession of smaller channels cross cutting one another. The southwest end of the southern may contain a thief zone, probably water saturated McMurray Formation sands. This interpretation was further supported by combining the amplitude anomaly distribution map with semblance time slices. The northern anomaly was observed to coincide with Lower McMurray Formation channels, where the distribution of steam appeared to be bound by the edge of a mud-filled channel contained within the larger McMurray Formation channel feature.

The area outside of the two large McMurray Formation channels was interpreted to be dominantly mud and shale, with interspersed sand. These muds and shales create baffles to steam flow, preventing heat flow and thus bypassing sand units not contained within the two large channels.

Through each of the interpretation techniques employed, a detailed distribution of steam anomalies and time-delays were presented in a spatial display. The integration of geological well logs, and the co-integration of interpretation techniques (e.g. semblance

time slices with amplitude anomaly distribution maps) provided robust interpretations for the distribution of steam anomalies. The anomalies were observed to be located within large channel features of the McMurray Formation, bound by muddy IHS and restricted in some regions by thief zones. Overall, the majority of the steam was observed within two large McMurray Formation channels, comprised of an amalgamation of smaller channel features.

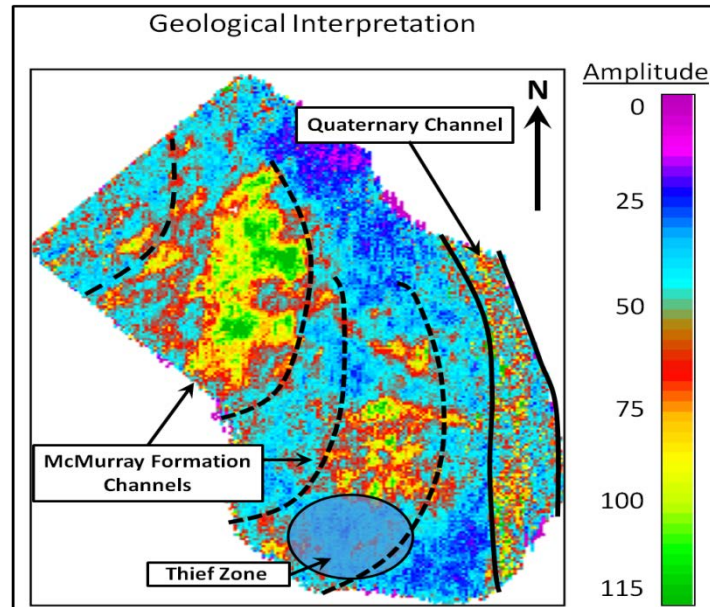


Figure 30 Combined geological and geophysical interpretation of two McMurray channels, with interpreted boundaries overlain on amplitude anomalies

ACKNOWLEDGEMENTS

Thanks to my supervisor, Dr. Don Lawton for his support and advisory. Thank you to the CREWES sponsors for sponsoring this work, as well as the CREWES students, faculty and staff. Thank you to the industry donor of the data, as well as to Helen Isaac for her help processing the data.

References

- Barnes, A. E., 2007. A tutorial on complex seismic trace analysis. *Geophysics*, 72(No. 6), pp. W33-W43.
- Chopra, S. & Marfurt, K., 2008. Gleaning meaningful information from seismic attributes. *First Break*, Volume 26, pp. 43 - 53.
- Chopra, S. & Marfurt, K. J., 2007. *Seismic attributes for prospect identification and reservoir characterization*. Tulsa, Oklahoma: Society of Exploration Geophysicists.
- Clifford, P. J. et al., 2003. Integration of 4D seismic data into the management of oil reservoirs with horizontal wells between fluid contacts. *Society of Petroleum Engineers* 83956, pp. 1-10.
- Drijkoningen, G. et al., 2012. Seismic time-lapse effects of solution salt mining - a feasibility study. *Geophysical prospecting*, Volume 60, pp. 239-254.
- Eastwood, J., 1993. Temperature-dependant propagation of P- and S-waves in Cold Lake oil sands: Comparison of theory and experiment. *Geophysics*, 58,(No.6), pp. 863-872.
- Eastwood, J. E. et al., 1998. Processing for robust time-lapse seismic analysis: Gulf of Mexico example, Lean Field. *68th Annual International Meeting, Society of Exploration Geophysicists, Expanded Abstracts*, pp. 20-23.
- Eastwood, J., Lebel, P., Dilay, A. & Blakeslee, S., 1994. Seismic monitoring of steam-based recovery of bitumen. *The Leading Edge*, 13(4), pp. 242-251.
- Eiken, O., Haugen, G. U., Schonewille, M. & Duijndam, A., 2003. A proven method for acquiring highly repeatable towed streamer seismic data. *Geophysics*, 68(No.4), pp. 1303-1309.
- Gadallah, M. R. a. F. R. L., 2005. *Applied Seismology. A comprehensive guide to seismic theory and application*. Tulsa, Aklahoma: PennWell Corporation.
- Hampson-Russell, n.d. *Hampson-Russell Guide*. s.l.:s.n.
- Hickey, C., Eastwood, J. & Spanos, T. J., 1991. Seismic wave propagation in oil sands. *AOSTRA J. Res.*7, pp. 67-81.
- Hien, D. H., Jang, S. & Kim, Y., 2010. Multiple seismic attribute analyses for determination of bottom simulating reflector of gas hydrate seismic data in the Ullung Basin of Korea. *Marine Geophysical Researchers*, pp. 121-132.
- Isaac, J. H., 1996. *Seismic methods for heavy oil reservoir monitoring*, Calgary: University of Calgary, Department of Geology and Geophysics.
- Johnston, D. H., 1997. A tutorial on time-lapse seismic reservoir monitoring. *Offshore Technology Conference*, pp. 141-146.
- Johnston, D. H., 1997. A tutorial on time-lapse seismic reservoir monitoring. *Journal of Petroleum Technology*, 49(5), 473-475, pp. 473-475.
- Kalantzis, F. V. A. K. E. R. K. A., 1996. Seismic monitoring and modeling of an enhanced oil recovery project at Cold Lake, Alberta, Canada. *Canadian Journal of Exploration Geophysics*, vol 32, no. 2, pp. 77-89.
- Kommedal, J. & Barkved, O. I., 2005. 4D repeatability beyond twice - using variance. *Society of Exploration Geophysicists Expanded Abstracts*, pp. 2526-2529.
- Koster, K., Gabriels, P., Hartung, M. & Verbeek, J., 2000. Time-lapse seismic surveys in the North Sea and their business impact. *The Leading Edge*, v.19(No.3), pp. 286-293.
- Kragh, E. & Cristie, P., 2002. Seismic repeatability, normalized rms and predictability. *The Leading Edge*, 21(No.7), pp. 640-647.
- Macrides, C. G. & Kanasewich, E. R., 1987. Seismic attenuation and poisson's ratios in oil sands from crosshole measurements. *Canadian Society of Exploration Geophysicists*, 23(No. 1), pp. 46-55.
- Marfurt, K. J. et al., 1999. Coherency calculations in the presence of structural dip. *Geophysics*, Volume 64, pp. 104-111.
- McGillivray, P., 2005. Microseismic and time-lapse seismic monitoring of a heavy oil extraction process at Peace River, Canada. *Recorder*, pp. 5-9.
- Nakayama, T., Takahashi, A. & Kato, A., 2008. Oil sands reservoir monitoring using time-lapse 3D seismic in canada. *International petroleum technology conference*, Volume 12333.
- Nakayama, T. T. A. S. L. a. K. A., 2005. Monitoring an oil-sands reservoir in northwest Alberta using time-lapse 3D seismic and 3D P-SV converted wave data. *The Leading Edge*, pp. 1158-1175.
- Nur, A. M., 1982. Seismic imaging in Enhanced Recovery. *SPE/DOE 10680*, pp. 1-11.
- Riedel, M., Collett, T. S. & Shankar, U., 2011. Documenting channel features associated with gas hydrates in the Krishna-Godavari Basin, offshore India. *Marine Geology*, Volume 279, pp. 1-11.
- Robinson, E. A. & Treitel, S., 2000. *Geophysical signal analysis*. s.l.:Society of Exploration Geophysicists.

- Rojas, N., 2008. Spectral decomposition applied to time-lapse seismic interpretation at Rulison Field, Garfield County, Colorado. *Colorado School of Mines Dissertation*.
- Schmidt, J., 1990. Seismic detection of porosity in the Tensleep sandstone reservoir, South Casper Creek, Wyoming. *Colorado School of Mines, Dissertation*.
- Schmitt, D. R., 1999. Seismic attributes for monitoring of a shallow heated heavy oil reservoir: A case study. *Geophysics*, 62(No. 2), pp. 368-377.
- Sheriff, R. E., 2002. *Encyclopedic Dictionary of Applied Geophysics*. Tulsa: Society of Exploration Geophysicists.
- Taner, M. T., Koehler, F. & Sheriff, R. E., 1979. Complex seismic trace analysis. *Geophysics*, 44(No.6), pp. 1041-1063.
- Tanner, 2002. *Attributes revisited: Technical paper in rock solid images*. [Online] Available at: <http://www.rocksolidimages.com/pdf/attribrevisited.htm>
- Wang, Z. & Nur, A., 1988. Effect of temperature on wave velocities in sands and sandstones with heavy hydrocarbons. *Borehole Geophysics*, Volume 1, pp. 3-5.
- Watson, A. I., 2004. *Integrated geological and geophysical analysis of a heavy-oil reservoir at Pikes Peak, Saskatchewan*, Calgary, Alberta: M.Sc Dissertation, University of Calgary.
- Yilmaz, O., 2001. *Seismic Data Analysis. Processing, Inversion and Interpretation of seismic data..* Tulsa, Oklahoma: Society of Exploration Geophysics. .
- Yuwen, C. T. P. L. W. a. Y. L., 1998. Monitoring steam injection performance in shallow heavy oil reservoirs. *Proceedings - UNITAR International Conference on Heavy Crude and Tar Sands*, 7, No. 1998.108, pp. 1-9.